Anion-π and lone pair-π interactions with *s*-tetrazine-based ligands

Matteo Savastano,[a] Celeste García-Gallarín,[b] Maria Dolores López de la Torre,[b] Carla Bazzicalupi,*[a] Antonio Bianchi,*[a] Manuel Melguizo*[b]

[a] Department of Chemistry "Ugo Schiff", University of Florence, Via della Lastruccia 3, 50019 Sesto Fiorentino, Italy

[b] Department of Inorganic and Organic Chemistry, University of Jaén, 23071 Jaén, Spain

* Corresponding authors

Abstract

Most of traditional and contemporary interest in *s*-tetrazine derivatives focuses onto their redox properties, reactivity and energy density. In recent times, however, an increasing number of reports highlighted the possible usefulness of the *s*-tetrazine moiety as a binding site for anionic and electron rich species, according to the high and positive quadrupolar moment of this heterocycle and the consequent strength of anion-π and lone pair-π interactions. Herein, after giving a quick perspective on *s*-tetrazine properties and on how they foster these types of π interactions, we present statistical and critical examination of the available structural data, doing justice to the debated topic of the existence and directionality of anion- and lone pair-π interactions. Finally, available literature material concerning the usage of *s*-tetrazine as supramolecular binding site in solution, i.e. paving the way to applications such as molecular recognition and sensing, is presented and discussed.

Contents

1. Introduction

The lone pair-π [1-7] and anion-π [1, 8-19] interactions are emergent noncovalent forces whose occurrence has recently been recognized in both synthetic architectures [8, 20, 21] and biomolecular structures [4, 22-26] and are now taken into account for the construction of new functional materials [27-34], receptors [35-43] carriers [44-50], catalysts [51-57], and sensors [3, 34, 58-66].

While cation-π and hydrogen-π interactions can be easily rationalized on the basis of electrostatic considerations, the generation of a stabilizing effect from the interaction of anions, or lone pairs of electrons, with the π electron system of an aromatic ring appears counterintuitive, since common aromatic rings, like benzene, are characterized by negative quadrupole moments. These quadrupole moments, however, can be inverted either upon insertion of strongly electron-withdrawing substituents or heteroatoms able to accumulate more positive charge towards the ring centre, turning parent aromatic systems into π-acids able to form attractive interactions with anions as well as with not-charged atoms bearing lone pairs. Further contributions, such as polarization effects, dispersion forces and charge transfer (CT) can accompany the electrostatic component in the formation of anion-π and lone pair-π interactions [1-3, 11, 17, 18, 22, 67-70].

Replacement of the C atoms in 1,2,4,5 positions of benzene with four N atoms, to formally generate the *s*-tetrazine ring, introduces a perturbation in the electronic structure of benzene that generates peculiar characteristics such as a marked electron deficiency, a positive value of the quadrupole moment and a relatively high value of the polarizability perpendicular to the ring plane. Accordingly, *s*-tetrazines are able to form anion-π and lone pair-π interactions, as substantiated by the significant number of crystal structures analysed in this review.

We have recently studied some functionalized *s*-tetrazines and observed a particular propensity of these molecules to form both anion-π and lone pair-π contacts [71-77]. We also found that these molecules can function as receptors for anion binding in solution where they form anion complexes which are stabilized by anion-π interactions, generally in conjunction with other weak forces [71-76].

Our interest in the anion-π and lone pair-π binding properties of *s*-tetrazine-based molecules encouraged us to perform the search of information and the analysis of data that are collected in this review. Most evidence of such interactions comes from crystallographic data and, accordingly, the main section of the review deals with the analysis of crystal structures made available by the Cambridge Structural Database (CSD). Given the controversy concerning relevance and occurrence of these interactions for benzene and few prototypical heterocycles, partly due to the disagreement in geometric parameters used to survey data banks such as CSD (cf. section 3.1), we devoted ourselves to propose an assumption-free search routine to locate all contacts found between the *s*-tetrazine rings and the electronegative atoms N, O, F, P, S, Cl, Br and I, whether negatively charged or lone pairs. These data were then considered and analysed both as a single set and as separated groups including, respectively, data for anions and for lone pairs.

This section will be preceded by a brief review of the synthetic procedures adopted for the preparation of *s*-tetrazine derivatives and of the main chemico-physical properties and applications of these compounds and will be followed by a summary of the still modest set of information on the anion-π interactions that these compounds also appear to form in solution.

2. s-Tetrazine Synthesis & Properties

2.1. Synthesis of *s*-tetrazine derivatives

s-Tetrazine derivatives are known from the early work of Pinner, more than one century ago, [78,79] who originally proposed the treatment of imidates with excess of hydrazine to produce dihydro-1,2,4,5-tetrazines which, upon oxidation, afford the fully aromatic *s*-tetrazine. Since imidates were obtained by alcoholysis of the corresponding nitriles (the so called Pinner reaction) [80], the most extended procedure for the synthesis of *s*-tetrazines became the treatment of nitriles with hydrazine and a catalyst (commonly a protic or Lewis acid, or elemental sulfur), in an alcohol as solvent, to give the intermediate dihydrotetrazine, that is subsequently aromatized by treatment with an oxidant (Scheme 1).

Scheme 1 to be inserted about here.

Though other routes are also known, the Pinner synthesis continues been up today the main procedure employed to prepare *de novo* *s*-tetrazine aromatic rings. The literature devoted to the synthesis of *s*-tetrazines has been the subject of several good reviews [81-84], so that we will only briefly comment here some of the last interesting innovations that improve the classical Pinner synthesis and its scope, so widening the number of derivatives available to the blossoming field of *s*-tetrazines' applications. Thus, the use of N-acetylcysteine [71,85,86] and other thiols [87] as catalysts (instead of elemental sulfur), and of atmospheric air as a green, mild oxidant to transform dihydrotetrazine intermediates into the aromatic derivatives are noteworthy improvements that afford good results under milder conditions [85,71,88–90]. Together with them, the incorporation of dichloromethane as a one-C fragment to synthesize 3-monosubstituted tetrazines [91] can be considered one of the most relevant novelty.

Concerning the modification of substituents at the carbons C(3)/C(6) after tetrazine ring formation, the availability of 3,6-dichloro-*s*-tetrazine [92] constituted a true landmark in the field owing to the great potential of this compound to generate a vast diversity of substitution patterns, both symmetrical and unsymmetrical, by aromatic nucleophilic substitution of the chlorine atoms [93-95], as well as by other ways such as Pd-catalyzed C-C coupling reactions [96-97]. Other advances, of particular interest in the field of energetic and explosive materials, are the new procedures introduced to prepare mono- and bi-N-oxides of the *s*-tetrazine nucleus [98-99].

2.2. General perspective on the properties and applications s-tetrazines

It was just in recent times, practically coinciding with the change of millennium, that *s*-tetrazines have attracted a more general interest in the scientific community by virtue of their particular properties and their great potential in diverse applications. Figure 1 is an attempt to outline the relationship between the

main structural features of the *s*-tetrazine nucleus and some of the measurable properties showed by its derivatives which, in turn, constitute the basis of their potential applications.

Figure 1 to be inserted about here.

According to Figure 1, we consider three structural features as fundamental to describe the most relevant properties displayed by *s*-tetrazine derivatives:

a) A π* LUMO of relatively low energy, spatially restricted on the *s*-tetrazine ring. According to molecular calculations [97,101-104], this is a general feature of *s*-tetrazine derivatives, regardless of the substituents connected to C(3) and/or C(6) (unsaturated and aromatic included), though the nature of the substituents obviously influences the orbital energy. The electron transitions $n \rightarrow \pi^*$(LUMO) that take place by absorption of light of wavelength around 530 nm, with low molar adsorptivities (typically, $\varepsilon \approx 600$ L·mol^{-1}·cm^{-1}) [81,94,97] due to symmetry mismatch between the orbital involved, are responsible for the characteristic colour (red-pink-purple) of the *s*-tetrazine derivatives.

b) A marked electron deficient character (due to the incorporation of four nitrogen atoms into the 6-membered aromatic ring of *s*-tetrazine), as clearly showed by the electrostatic potential calculations [100,105].

c) A positive value of the quadrupole moment (Q_{zz} = +2.5 B; 1B = 3,336·10-40 C·m^2) [100] and a relatively high value of the polarizability perpendicular to the ring plane ($\alpha_{\perp} \approx 33$ a.u.). [106] These two features are taken together because they are the more direct responsible for the favourable anion-π and lone pair-π non-covalent interactions involving *s*-tetrazines (cf. section 2.3).

Redox properties undoubtedly are amongst the most interesting attributes of *s*-tetrazines (Tz) concerning their potential applications in new functional materials. In particular, it is well known their capacity to capture an electron to give a radical anion, $Tz^{\cdot-}$ [81]. This is a reversible process related to two of the most relevant structural features of the *s*-tetrazine nucleus just commented: the existence of a LUMO cantered on the *s*-tetrazine ring, and the marked electron-deficiency of said ring. The reversibility of the electron capture to give a radical anion ($Tz + e^- \leftrightarrows Tz^{\cdot-}$), and that of *s*-tetrazine reduction upon receipt of two electrons and two protons ($Tz + 2e^- + 2H^+ \leftrightarrows H_2Tz$), grant *s*-tetrazine derivatives a clear ability to be employed in the preparation of organic conductors and semiconductors for electronics [88,107,108] and photovoltaics [97,109,110], electroluminochromic [111] and electrofluorescent materials [112,113], photocatalysts [114] or electroactive materials for secondary batteries [115].

The recognition of s-tetrazine derivatives as substances of interest in the formulation of explosives and pyrotechnics produced one of their earliest applications. The value of *s*-tetrazines in this field stems from the high N/C ratio of the aromatic nucleus, that can be further increased by connecting suitable substituents (hydrazine, guanidine, tetrazole, …) to its C(3)/C(6) carbon atoms. Also, the planar character of

the aromatic *s*-tetrazine ring enables compact molecular packings which are essential to realize substances with a high (volumetric) energy density [116,117]. This is a field that continues very active in seeking for new *s*-tetrazine derivatives of interest [118-120].

Other important applications of *s*-tetrazines derive from their particular reactivity, that serves as the base of the usefulness that these structures are proving in molecular biology studies, as reacting partners in *bioorthogonal chemistry* [121] methods (a field that has boosted the research and literature devoted to *s*-tetrazines from the first 2000s) [84,122]. These applications take advantage of two properties of *s*-tetrazines: i) the propensity of the *s*-tetrazine nucleus to act as 2,3-diazadiene in fast inverse-electron-demand Diels-Alder (iedDA) reactions with alkenes and alkynes that affords, in a first term, a bicyclic adduct which immediately suffers a retro-Diels-Alder (rDA) reaction, evolving N_2, to give rise to dihydropyridazines or aromatic pyridazines, respectively (Scheme 2) [123,124]; ii) the inertness of s-tetrazine derivatives towards natural substances under biological conditions.

Scheme 2 to be inserted about here.

But the property that focused our interest in *s*-tetrazines, and constitutes the main subject of this review, is their ability to establish non-covalent bonds to negatively charged species (anion-π bonds) or atoms with non-shared electron pairs (lone pair-π bonds) located over the ring plane in the proximity of the ring centroid. This property enables *s*-tetrazine derivatives to find application in the field of sensors and receptors [65], as well as to act as directors of molecular conformation and molecular assembly [125-126], which, in turn, can be exploited in the design of new catalysts [51,127].

2.3. Anion-π and lone pair-π: nature of the interactions and relevance of the *s*-tetrazine ring

At first sight, an attractive interaction between anions and the aromatic *s*-tetrazine through one of its ring faces (where the clouds of the delocalized π electrons are located), can appear counterintuitive. However, the pioneering studies by Deyà and Frontera [67,105], who had previously coined the term "anion-π bond" [16], clearly pointed out that the *s*-tetrazine system possesses suitable features to give this type of non-covalent interactions. Their calculations evidenced that the electron density on *s*-tetrazine is characterized by a molecular electrostatic potential with a concave shape over the ring faces, with more positive values around the ring centre, that would favour electrostatic interactions with negatively charged species placed over the ring plane. Their models of interaction between *s*-tetrazine and halide anions (F^-, Cl^- and Br^-) showed the stabilization of anion-π bonds [105]. According to their analyses, the main component of this interaction was considered to be of electrostatic nature and depended directly on the quadrupole moment, Q_{zz}, of the aromatic ring [128]. At that time, several X-ray diffraction studies of metal complexes involving *s*-tetrazine ligands confirmed a key role of anion-tetrazine interactions in the stabilization of the crystalline structure [125,126,129,130], in support of the ability of *s*-tetrazine ring to participate in anion-π non-covalent bonds.

Though some debate around the nature of the anion-π bonds still lasts, a certain accord exists on the fact that there are three main components that contribute to the total energy of the interaction [3, 131, 132]:

one is due to the electrostatic attraction between the negative charge of the anion and the electric quadrupole of the aromatic ring; the second is a polarization component arising from the interaction between the anion charge and the electric dipole induced by this charge on the electron π-cloud of the aromatic ring; and the third is the dispersive component, always attractive. About a possible contribution of charge transfer to the anion-π bond stabilization, the results given by theoretical calculations can be controversial owing to their essential dependence on the calculation method [11]. In general, it is mostly accepted that the contribution of charge transference to the energy of the anion-π bond is negligible [131,132], though there are some reports that claim a large character of charge transference for some particular anion-π complexes [133].

Analysing in more detail the contributions to the energy involved in anion-π interactions, and firstly concerning the electrostatic component, the suitability of π systems to bond to anions is determined by their quadrupole moment, Q_{zz}, so that systems with a positive value of Q_{zz} interact attractively with anions, while those with negative value of Q_{zz} do it with cations (i.e. are inherently suitable to form cation-π bonds) [11,16,25,134]. For instance, benzene, with a Q_{zz} = -8.5 B, is capable of participating in cation-π interactions, while hexafluorobenzene, recognized as a typical π-acid with an excellent ability to participate in anion-π bonds, possesses a quadrupole moment of Q_{zz} = +9.5[135]. About the dipolar component of the bonding energy, it depends on the deformation induced by the anion charge on the π cloud of the aromatic systems, that, in turn, is a function of its polarizability in the direction perpendicular to the ring plane, $\alpha_{\perp}$ [11,67,136]. The third bond energy component, i.e. the London dispersive forces [137], are also a function of the polarizability of the π system and their contribution to the interaction energy, according to recent measurements of the energy of anion-π bonds in gas phase [131], seems to be larger than what was previously considered. Then, it is not only the quadrupole moment, but also the polarizability of the π system that have a prominent role in determining the strength of the anion-π bonds. This leading function of the polarizability has gained recognition from some recent experimental works where handling the polarizability of aromatic systems by means of π-stacking [138-140] or external electric fields [141] were used to favour anion-π interactions and made them useful in recognition of anion species or even in catalysis [51]. In agreement with these strategies for strengthening of anion-π interactions through polarization modification, an exhaustive revision of the occurrence of anion-π interactions in biomolecules [26] shows how modification of the polarization of aromatic rings is an extended strategy in biomolecules, such as proteins, DNA or RNA, to fortify anion-π non-covalent bonds working for conformation stabilization [24,142].

Even if it is properly not a part of the nature of the anion-π bond itself, the solvent plays a fundamental role in the energy balance of the bond formation from the implicated species, anion and π system. The literature contains a small number of experimental thermodynamic studies on formation anion-π complexes in solution but, all of them point out that in polar solvents, as acetonitrile or water [71,73,143-145], there is a relevant favourable entropic contribution to the complex stabilization energy (yet with some particular exception) [73]. In general terms, this behaviour parallels that observed in the formation of ionic pairs in solution [146], and can be attributed to the need of releasing solvent polar molecules, highly organized around the ionic or polar species, to reach complex formation (Equation 1).

$$(\pi)[Solv]_n + (A^-)[Solv]_m \leftrightarrows (A^-/\pi)[Solv]_{(m+n)-x} + x\ Solv \quad (1)$$

π = ligand based on a π system; A^- = anion; (A^-/π) = anion-π complex; Solv = solvent molecules.

It is in this context that the capacity of the *s*-tetrazine system to form anion-π complexes will be discussed. Then, calculations on the quadrupole moment of *s*-tetrazine systems give a positive value of the quadrupole moment, Q_{zz} = +2.5 B [100], clearly higher than those of other recognized π-acidic molecules, such as *s*-triazine (+0.3 B) [100] or 1,3,5-trifluorobenzene (+0.5 B). [147] These data confirm the π-acidic character of *s*-tetrazine and makes it intrinsically suitable to form anion-π bonds [11]. Additionally, the *s*-tetrazine ring possesses a significant value of polarizability perpendicular to the ring plane, $\alpha_{\perp} \approx 33$ a.u. (and average polarizability of ≈ 50 a.u.) [106,148-151], that also favour its ability to participate in anion-π non-covalent bonds. Although its quadrupole moment and polarizability are not so high as those of other fused aromatic systems, as naphthalenediimide or perylenediimide [139], the smaller size of *s*-tetrazine (a 6 member ring with only two substituted positions) favours its solubility in water and makes it more appropriate to be used in aqueous systems, where entropically favourable desolvation effects can help to strengthen tetrazine-anion complex stability [10].

The features commented above also qualify *s*-tetrazine derivatives to participate in lone pair-π non-covalent interaction, where a neutral chemical species employs a non-shared electron pair to stablish a stabilizing interaction with one of the faces of a π-acid [1,152]. The parallelism of lone pair-π with the anion-π interactions are evident, as are too their differences. The charge neutrality of the species that provides the non-shared electron pair ensures that the polarization and dispersive components will be larger than the electrostatic component of the global interaction energy, which, in turn, will be generally smaller than that of the corresponding anion-π interactions (at least when aromatic systems with a marked π-acidity are involved) [153-155]. In spite of its intrinsically weak character, the participation of *s*-tetrazines in lone pair-π interactions with non-shared pairs of oxygen and nitrogen atoms in solid phases have been evidenced by x-ray crystallographic studies [73].

3. Anion-π and lone pair-π interactions with *s*-tetrazines in the solid-state: CSD Survey

An evaluation of all contacts found in the Cambridge Structural Database (CSD) between the *s*-tetrazine ring and the electronegative atoms N, O, F, P, S, Cl, Br and I, whether bearing a negative charge or lone pairs, has been carried out.

Data have been organized in several different sets: data for anion and lone pair interactions with the π system of the *s*-tetrazine will be analysed together and separately, both using 2D projection and 3D distributions.

Employed van der Waals radii, according to Alvarez recent update [156], are reported in Table 1.

Employed methodology and its explanation is given in detail in the *3.1. Methodology and rationale of the survey* section, while results are presented in the *3.2. Structural data analysis* section.

Table 1 to be inserted about here

3.1. Methodology and rationale of the survey

Our first concern is to define what we consider as a hit.

This may seem a trivial point, but it is the single most important part of a CSD survey. Assuming a deterministic relationship between the raw aggregated data extracted from the database and the published elaborated data, the black box determining the quality of the results is indeed just the used query. Referring to everyone's experience, the Analytical Chemist would say that, as long as we can make accurate measurements, results are already determined once we have a sample in our hands; yet, if the sampling was poor from the beginning (i.e. it is not representative), the analysis is doomed to be biased.

The main source of bias in CSD surveys arguably comes from our own prejudice: if we think data should behave in a particular way, we tend to set up queries which magnify exactly what we are interested in investigating. What we should do instead is collecting all sensible information in the most result-neutral way, then use a statistical approach to discern whether our working hypothesis was correct or not. In the present case, we intend to demonstrate that anion-π and lone pair-π interactions are respectively pivotal and contributing to the stabilization of *s*-tetrazine complexes. To accomplish this, we will first locate all anion/lone pair contacts with the *s*-tetrazine ring and then analyse their overall spatial distribution to check if the working hypothesis hold.

Several CSD surveys locating anion or lone-pair contacts around arenes had been previously performed. Figure 2 presents a graphical comparison of the sampled areas in the current and previous surveys: as one can easily see there are significant differences among them, affecting the final quality of the data. Beyond graphics, it is important to understand the evolution of the rationale of these inquiries.

Figure 2 to be inserted about here.

First examples had sampling areas biased towards the centroid as a mean to hunt and highlight anion-π interactions (blue area Figure 2a) [7]. This however led to the artificial picture of them as almost ubiquitous and prominent interactions due to the bias towards the centroid. Large spherical distributions (5-6 Å from the centroid) were later employed as a simple tool to avoid bias towards the centroid (green area Figure 2b) [157], with the adverse effect of biasing towards the edge instead. This is manifest in hits or counts vs radius plots, where the cubic scaling of the sampled volume at higher radii necessarily results in more hits at the periphery. Moreover, long contacts generally carry less and less chemical sense at higher radius: an anion or lone pair right above an arene centroid and 3 Å away from it is probably there for a reason, while one in the same position but 5 Å apart has nothing to do with anion/lone-pair-π interactions. Some adjustments, i.e. combining a spherical sampling with other simple constraints (e.g. angular value limits),

have been proposed as a screening way to identify meaningful contacts with light queries on large datasets (eg. PDB) (Figure 2e) [26]. Other studies, questioning early centroid-biased results, proposed a model based on a large spherical sampling trimmed by an ellipsoid approximating the size of the arene but 1 Å thicker (red area Figure 2c) [158]. This is perhaps the closest sampling strategy to the one we present in this review (yellow area Figure 2d). However, neglecting the geometrical differences (see below), It is important to understand that the ellipsoid model fulfils a different conceptual role: it somewhat sacrifices a little bit of strict chemical significance, in the sense of being an imperfect approximation of the arene, to gain the status of an easy to manipulate mathematical object. This is significant for statistical purposes as it can and has been used to compare CSD experimental datasets with theoretical random scattering [158].

Our aim, beyond objectivity of the data, is to discuss the reasoning behind data collection and do it in a way that can be easily understood and replicated by the broadest audience possible: other equivalent possibilities exist [11] and will be discussed (see the discussion relative to Isostar software below), but they seem less fit for a thorough discussion. Furthermore, we would like to present a methodology which could be potentially translated to any possible heterocycle and to any class of anions/lone pair bearing atoms. As such, we would rather not rely on approximations based on geometry (e.g. an ellipsoid approximation for an arene is much more fitting for benzene than for the generic heterocycle, which, due to its nature, necessarily possess one or more chemically and spatially different positions) and have case-specific criteria depending on the nature of the anion.

In our refined model, a hit was counted when it satisfied all the following criteria, applied in order (point by point explanation follows):

1. An atom Z (Z = N, O, F, P, S, Cl, Br, I) is found (for Conquest: contact, intermolecular) within a 6.5 Å distance from the centroid of an *s*-tetrazine ring;

2. said atom is also found within a distance $d_1(Z)$ from the centroid, with $d_1(Z) = d_{\text{Centroid-Furthest Ring Atom}} + vdW_C + vdW_Z + \text{margin}$;

3. said atom is also found within a maximum distance $d_2(Z)$ from the mean plane of the tetrazine, $d_2(Z) = vdW_C + vdW_Z + \text{margin}$;

4. said atom is also in contact with at least one of the atom of the ring within a distance $d_3(Z)$ or $d_4(Z)$, $d_3(Z) = vdW_C + vdW_Z + \text{margin}$ and $d_4(Z) = vdW_N + vdW_Z + \text{margin}$, with $d_3(Z)$ and $d_4(Z)$ used for C and N ring atoms respectively.

A breakdown of the sampled area is shown in Figure 3.

Figure 3 to be inserted about here

The rationale of this choice goes as follows.

First, a generic spherical survey is executed, sampling distances from the centroid far higher than any possible $d_1(Z)$, namely at 6.5 Å (i.e. bigger than $d_1(Z)$ with Z = I) to avoid loss of any interesting contact.

In second instance, an element-specific spherical sampling was performed using $d_1(Z)$ as the upper limit of the distance from the centroid. Within $d_1(Z)$ we inserted a margin value: this is the only arbitrary parameter, which is adjustable to tastes or needs of the specific survey. We decided to set said margin to 0.5 Å for the present work. This value of margin allows to cut most of the unwanted noise while retaining the capability to locate a meaningful amount of contacts at the periphery of the ring. This allows for example to distinguish over- or under-populated areas in the ring plane arising from the formation of C-H-anion/lone pair contacts or steric hindrance by ring substituents (see 2D and 3D distributions discussion below). The only other possible disagreement might be on the constant value used for the Centroid-Furthest Ring Atom distance: we adopted 1.4 Å, as if tetrazine did not differ much from benzene (real values from CSD: Centroid-C = 1.28 ± 0.02 A, Centroid-N = 1.36 ± 0.02 A). If anyone feels that said value should be increased or decreased by few hundredth of Å, the survey can be regarded as performed with a slightly more generous or tight arbitrary margin compared to the said 0.5 Å.

The third step, i.e. imposing a $d_2(Z)$ distance from the ring plane, is superfluous as it is implicitly included in the fourth step: yet we find it to be valuable for discussion (in truth this constrain also speeds up data handling by discarding a large number of hits lacking proper contact with the arene). As anticipated above, spherical distributions are not an unbiased way to evaluate contacts because a lot of unspecific, if not non-existing contacts, are found at high radius values, hence the need of cutting and/or selecting the data of interest. This is particularly evident for arenes in terms of distance from the plane. Looking at Figure 3, all the blue circle area is within $d_1(Z)$ from the centroid, but only the area within the orange square is within $d_2(Z)$ from the plane (i.e. within the sum of vdW radii of C + Z + 0.5 Å, C vdW radius used as C is the bulkier atom in *s*-tetrazine.): all the rest of the blue circle in Figure 3 is just oversampling, as no chemical interactions exists between the partners. Ensuring the effective Z-ring contact within a reasonable distance appears as a rational decision.

In accordance to this very same principle, i.e. avoiding the sampling of areas in which chemically meaningful contacts between anion/lone pairs and arene are non-existent, we included the fourth constrain: each anion/lone pair must be in contact with at the very least one of the atoms of the ring within a maximum distance equal to the sum of the van der Waals radii of the atoms in contact (hence the difference between $d_3(Z)$ and $d_4(Z)$, for the C and N atoms of the ring respectively, please note that in our case $d_3(Z) = d_2(Z)$ because C is also the ring atoms with the bigger vdW radius) plus the set margin (0.5 Å). This means requiring that a short contact must exist within the anion/lone pair and one of the atoms of the ring, else there is no reason to question if the two are interacting: they simply are not. If we look again at Figure 3, the blue sphere area within the orange square (constrains at point 3, see above) which does not overlap with the yellow circles (depiction of the constrain 4) does not interact at all with the arene, thus all the hits eventually falling in this region of space should be discarded. Someone may think that the difference is negligible: it is not. A percentage in the 20-30% of the total hits can easily fall in the region discarded by constrain 4, refer to Figure S1 for an illustrative case in-point.

What is then the shape of the sampling area used in the current CSD survey?

The best way to visualize it is thinking about it as a pumpkin featuring as many lobes or slices as there are atoms in the investigated arene, that is 6 lobes for *s*-tetrazine. Furthermore, such lobes are not identical, but they bulge outwards more or less depending on the vdW radius of the ring atom they refer to. This feature cannot be appreciated nor in Figure 3, as it was drawn for the prototypical benzene case (six symmetrical lobes), nor it is evident in Figure 2, as the lobate structure of the sampling area cannot emerge easily in 2D projections (although hinted at with the superimposition of yellow circles in Figure 3). This is also one of the features distinguishing the present CSD survey from others, [7,26,157,158] since in our case, differently from spheres or ellipsoids, there is non-sampled space in-between the lobes: the slight difference is appreciable in Figure 4 (again depicted for the benzene-chloride case) and in the eliminated contacts at low angle values in Figure S1. This approach locates all the possible hits around the target arene without favouring any region of space: preferences for centroid-Z interaction, CH···Z hydrogen bond-like contacts, η^2 type binding at the periphery of the ring and so on will be evaluated according to the statistical significance of the data, without inserting bias in the model used for the CSD survey which, as evident and pointed out elsewhere, [158] may cause serious misinterpretation of the data. As a final remark, the analysis can be readily extended to whatever ring-size or heteroatoms by applying the same considerations.

Figure 4 to be inserted about here

No other constrains upon data quality have been imposed. In principle, including only crystal structure of the upmost quality should always be of concern: in this framework, according to the scarce data available on *s*-tetrazines (430 total structures in the CSD), we rather preferred to use all the available information to make a more trustworthy statistical evaluation.

Furthermore, special care was used not to mix up anion and lone pair results, which are indeed chemical separated entities in the presented data. This is not a trivial point, because, as pointed out elsewhere, [7] most of the time such distinction gets blurred by the limit of the Conquest software itself. Although in the present case, due to the relatively small dataset (hundreds of hit), the work could have in principle be done by hand (and has indeed been checked so), relevant discussion and a set of automated adopted solutions are presented in the relative section of the Supporting Material, assisting the possible extension of the methodology to other arenes more represented numerically in the CSD.

Coordinate reference system and all relevant geometric parameters used in the analysis are defined in Figure 5.

Figure 5 to be inserted about here

Before we discuss the data, it is important to have in mind all the possible outcomes of the analysis and their meaning, lest we end up misinterpreting them. We can safely expect three main scenarios: *i*) one or more recognizable interaction patterns exist (hopefully anion-π and lone pair-π), and they are capable of affecting the distribution of hits around the *s*-tetrazine core; *ii*) the data does not show any particular behaviour; *iii*) the data are not conclusive.

The best-case scenario would be of course case *i*). What we may anticipate about it is that, should both anion-π and lone pair-π interactions be detected, anions are expected to give rise to much sharper and manifest effects, in accordance to the expected fading of electrostatic interactions while moving from properly charged species to dipolar ones.

Case *ii*), i.e. no trends observed, may be either indicative of bad sampling or truly signify the absence of forces capable to affect the overall hits distribution pattern. With a sampling of proper quality, Hay and Custelcean [158] used this instance to disprove the tendency of chloride anions to give rise to anion-π interactions with benzene in the solid state. Their sampling routine allowed to see an almost random scatter for positioning of $-CH_3$ groups around benzene, a centred distribution for the K^+ ion (owed to the cation-π interaction and demonstrating an appropriate sampling, i.e. one fit to show the chemical specificity of hits distribution) and a lack of any tendency to give centred interaction of the anion-π type for Cl^-, which was instead found preferentially forming C-H…anion contacts at the periphery of the ring. Credit also goes to their ellipsoid model: by using a very manageable object from a mathematic perspective, they could generate random distributions to be confronted with CSD data, an effective method to detect deviations from statistic behaviour.

Case *iii*), i.e. we may not draw a proper conclusion, could arise if the available CSD material is not enough to be of any statistical significance. This however may provide hints about the expectable magnitude of the interaction under investigation. Using once more the reported example of the benzene-chloride system, [158] it is extremely unlikely that anion-π interactions could possibly have passed unnoticed in Hay and Custelcean sample pool of 9082 contacts, unless the interaction itself is of abysmally small magnitude (or, in other words, there is no positive interaction at all). In the case of *s*-tetrazine the sampling pool is at least 1 order of magnitude smaller compared to the benzene-chloride system (cf. Tables 2 and 3). This means on one hand that there is an increased chance that the available crystal structures may not be representative of a statistical distribution and, on the other, that, should any interaction appear manifest, it should be of sizeable strength to be able to emerge even from a limited data set.

3.2. Structural data analysis

Let us start the discussion from the evaluation of the available material and the chemical identity of the interacting partners.

Of the 430 crystal structures containing the *s*-tetrazine ring, 379 (≈ 88%) present an atom Z (Z= N, O, F, P, S, Cl, Br, I) within 6.5 A from the arene centroid (thus satisfying only our first screening criteria). Of these, 112 (≈ 30%) are found in contact with anions fulfilling all our search criteria, giving rise to 618 contacts (≈ 5.5 average contacts per crystal structure), while 255 (≈ 67%) are found in contact with lone pair bearing atoms, generating 973 contacts (≈ 3.8 average contacts per crystal structure). This is in line with previous observations [7], where lone pair-π contacts have always been found more copious. The relevance of such remark, at least when used to affirm that such interactions are ubiquitous, clashes with the simple fact that lone pair bearing atoms are ubiquitous by themselves: finding them in contact with arenes is therefore

expected to be common and it does not necessarily imply the existence of any kind of specific interactions. A detailed overview of the species found is presented in Table 2 for anions and Table 3 for lone pair bearing atoms.

Tables 2 and 3 to be inserted about here.

As a first step, data have been analysed in terms of overall spatial and angular distributions: relevant plots are reported in Figures 6-10.

Figures 6-10 to be inserted about here

In terms of effectiveness of the devised search parameters, we may observe immediately from Figures 6 and 8 how anions and lone pairs tend to be distributed in arcs around the tetrazine ring according to their van der Waals radius. If we focus on the different curves drawn by F/O atoms (closest) and I/S ones (furthest) we must acknowledge that no search with a single fixed radius for all the possible interacting species is feasible (e.g. all simple spherical distributions), since if one of the two regions is sampled properly the other is doomed to be severely over- or under-sampled.

Cumulative angular distribution (Figures 7 and 9) clearly show that anions have a much more marked tendency to be located at high angle values (i.e. closer to the normal to the ring plane, viz. right above the *s*-tetrazine ring). This supports the thesis that electrostatic interactions with the quadrupolar moment of the arene should be stronger for anions than for lone-pair bearing atoms, however it is still not sufficient to affirm that anion- and lone-pair-π interactions are indeed at work. If we reverse the argument, limiting the search above a certain angle as in [26], does not grant to be sampling only species interacting through anion-π contacts.

The same kind of trend emerges from Figure 10: angular distribution of anions above the ring plane is more marked and with more definite features, with maxima around 60° and 75° and a significative percentage (≈ 10%) of hits located right over the centroid, i.e. in the 80-90° range. Although displaying analogous features, the trend for lone pair is considerably more blurred, and a significant percentage of hits is now distributed even in the low angle region.

A first hint about specific chemical interaction being at work is provided by the spatial distribution showed in Figures 6 and 8. Looking carefully, the sampled area above the ring centroid shows two distinct regions: a hit-dense zone close to the ring plane and a sampled-but-void area further from the plane. This pit has been highlighted for the more abundant data sets for both anion and lone pair bearing atoms in Figure 11. Such pits are again more marked for anions than for lone pair bearing species and show an interesting correlation with the calculated energy map reported for the interaction of F^- with *s*-tetrazine, Figure 12 [105] which shows a potential energy well right above the ring centroid.

Figures 11 and 12 to be inserted here

To give a definite answer on whether anion-π and lone-pair-π interactions with *s*-tetrazine based receptors are relevant forces, we were prompted to examine the 3D distribution of hits around this aromatic ring for both lone pairs and anions. For the sake of comparison, we opted to work with dataset possessing the same type of atom in contacts, choosing oxygen as a probe, as it accounts for a relevant number of hits for both anion (≈ 38% of total contacts) and lone pairs (≈ 36% of total contacts).

Projection of the resulting distributions are reported in Figure 13 for a whole face of the tetrazine (cf. discussion on 3d representation in the supporting material). As one can easily see, indeed most of the hits are located in the area close to the centroid, clearly showing an indentation towards the centroid spanning the whole ring along the C-C axis. Non-centred contacts, mostly belonging to the lone pair data set (in accordance to angular distributions in Figures 7 and 9), seem scattered evenly in all direction with the exception of the C-C axis, which appears almost devoid of hits. This is nor artificial nor indicative of any sort of interaction, instead it is a consequence of the fact that most (> 95%) of the available crystal structures belongs to the 3,6 disubstituted 1,2,4,5 tetrazine class: thus, the C-C axis at low angles cannot be populated by contacts because it is sterically blocked by the presence of substituents. A striking correlation emerges when the projection of the distribution in the xy plane (Figure 14) is compared with the electrostatic surface potential (ESP) of *s*-tetrazine (Figure 15). Both anion and lone-pair contacts distributions (shown separately in Figures 16 and 17) not only show a marked preference for hits to be located along the C-C axis, but also reproduce the overall X-shaped ESP potential of the *s*-tetrazine molecule. The high hit density observed above the centroid, not expected from ESP alone, was indeed correctly predicted by calculated interaction maps (cf. Figure 12, [105], and the analogous distribution of K^+ ion over the benzene ring in [158]). ESP directly correlates only with the electrostatic terms of anion and lone pair-π interactions (i.e. charge-ring quadrupole and dipole-ring quadrupole, respectively). Polarization effects and forces (i.e. charge-induced ring dipole and dipole-induced ring dipole, respectively), favouring centred interactions, are instead properly taken into account in the calculated interaction map (Figure 12), which justifies the observed hit density above the centroid. Given the supramolecular nature of both anion-π and lone pair-π interactions, the fact that experimental data distributions closely match the ESP of *s*-tetrazine, taking into account only the electrostatic contribution to the interaction, and perfectly mirrors finer calculations which include the polarization term, clearly indicates the existence of such forces. Considering the size of the available data set, it is surprising that such a detailed negative image of *s*-tetrazine ESP potential is reproduced by the 3D distributions of contacts.

Figures 14-17 to be inserted about here

On one hand, this may have to do with the quality of the performed sampling. A point worth mentioning once more is that clustering of data at the ring periphery, due to both cubic scale of spherical shell volume with radius and to the intrinsically diminished chemical sense the more we move far from the centroid (up to 5 Å in some literature cases) biases all simple spherical queries. The lobate structure of our sampled areas, with the seemingly petty difference showed for the equatorial plane in Figure 4, emerges in its full importance in the distribution displayed in Figures 16 and 17, where the lobes are clearly visible. Imagine now sampling a thicker spherical area instead, and for systems (e.g. benzene) which are far more

represented in the CSD: any interpretation of data distribution would be hindered by the large and unspecific noise of all the sampled non-interactions at the periphery.

On the other hand, this can be due to the intrinsic properties of the *s*-tetrazine core. This heterocycle is not only one of the most amenable to anion-π interactions [100], but also possesses a lower symmetry than many of the historically most investigated aromatic systems (benzene, its hexafluoro derivative, *s*-triazine, etc.). Such lowering of the overall symmetry together with the increased strength of the interaction probably contributes to our ability of detecting interaction patterns even from a limited dataset.

It should incidentally be mentioned that, at present, anion-π and lone-pair-π interactions with tetrazines are beyond the scope of the CCDC materials. The full interaction maps as implemented in the Mercury software are entirely based on the Isostar libraries. Such libraries, are records of all interactions found within the CSD with a selected ligand and a suitable probe, recording, for example, the position of alcohol OH (probe) around a protonated amino group (ligand). When generating full interaction maps, the structure under examinations is broken down into fragments (ligands), distribution of desired probes around all fragments is checked, and high probability density regions are highlighted with different shades and in different colours. This generates images suggesting the chemical and topological features that a possible substrate should possess to maximize its interactions with the target molecule, which can be invaluable for drug design and crystal engineering purposes. At present, *s*-tetrazines are not implemented. Following the stimulus provided by other papers in the field for such technical developments, e.g. demonstration for di- and tri-azines [11], which lead to their inclusion in the Isostar libraries, we auspicate that *s*-tetrazines will found equal consideration. Reliable predictions of supramolecular forces may radically change our approach at molecular screening.

Also, use of Isostar as a visualizing tool allowed Frontera and co-workers [11] to obtain 3D data of our same quality by simply performing a spherical distribution query and then visualizing only arene-anion contacts falling within the sum of their vdW radii: i.e. speeding up immensely the searching routine while also resulting in one of the top quality CSD surveys on the matter. That can always be done at the cost of setting up an in-house Isostar server and defining your own custom probes and ligand groups. We opted not to do so in this review, rather giving a rationale that everyone can freely use in simple Conquest searches, in an effort of keeping the discussion relevant for the broadest audience. However, if scholars working time is to be taken into account, prompt implementation of tetrazines among Isostar-supported systems is highly desirable.

Focusing on the data, anion contacts distribution possesses indeed much more marked features, as we could anticipate a priori: charged species being affected by electrostatic fields much more than dipolar ones. However, even when looking at distributions like those presented in Figures 13 and 14, this does not go beyond a qualitative observation. An attempt at a quantitative approach is shown in Figures 18-21, showing 3D wireframe/heat plot graphs showing the percentage distribution of hits around the *s*-tetrazine moiety as a function of the xy coordinates with respect to the ring plane. Eventually, should we think or prove that our distributions are fully representative, i.e. that they behave statistically, then these same plots can be thought of as showing the probability of a given O anion/lone pair bearing atom to be located in a certain region, i.e. they would allow to make those informed predictions which are crucial for drug design and crystal engineering purposes. It is most likely that the current available *s*-tetrazine crystal

structures do not show a perfect statistical behaviour yet, merely due to a matter of size of the dataset. However, we do not think that such a proof of statistical behaviour would add anything to the relevance of the results or their discussion for two main reasons. First, all informed predictions that we can possibly make derive from the gathered data: since at present there are no more data beyond those analysed in this review, predictions based on the displayed distributions are the more accurate that we can possibly make, statistical ensemble or not. Second, we already expressed the urge to implement this kind of interaction in the Isostar database: once a self-updating library exists, our predictions will automatically get better with each published crystal structure; so, once again, we might be using imperfect tools, but ones which will get more and more accurate over time.

Figures 18-21 to be inserted about here

What do we learn from these distributions?

Figures 18-21 have been prepared with the same 10 colours code, but, as shown in the legend, they refer to distinct percentages for anion and lone pairs. Anion distribution is indeed more peaked in general and especially towards the centroid, but now we are able to say, for example, that an O anion has a chance to be found in the 0.2 x 0.2 Å bin right above the ring centroid which is about 2.5 times the chance of finding an O lone pair bearing atom there.

There are plenty of things that can be learned by close inspection of Figures 18-21. One could for example compare the asymmetric potential well above the centroid calculated for fluoride (Figure 12) with the central part of Figures 19 and 21. Lone pairs show red probability areas with a definite shape and a maximum located right over the centroid: we are reproducing calculated interaction maps experimentally, with full 3D details. The pit for anions is much more populated and much more restricted to the C-C axis, at least for what concerns its highest probability area, in full agreement with ESP and calculated data.

It is also useful to compare Figures 19 and 17 and Figures 21 and 16. Someone may rest under the impression that these plots give the same kind of information, and although this is true to some extent, Figures 19 and 21 allow to perceive details which are not evident from the simple distributions of Figures 16 and 17. From Figure 21 we can clearly perceive that the area right above the tetrazine N atoms tends to be avoided by the anions, as expected from the molecule's ESP (Figure 15). Yes, there are a few hits there (Figure 16) but from a percent point of view they have a modest relevance.

Only a few contacts exist beyond a certain distance on the C sides of the ring, and we already mentioned that more than 95% of crystal structures contain 3,6 disubstituted *s*-tetrazines. Yet we could expect to see some clustering, i.e. some probability hotspots, close to the expected position for the C-H…O hydrogen bonds if they were a meaningful interaction. Contrary to the reported benzene chloride case [158], this does not seem to happen. On the contrary, despite the very low basicity of the aza-type N atoms of *s*-tetrazine, we can observe a certain tendency of lone pair bearing atoms to cluster at the periphery of the ring in position compatible with the formation of weak hydrogen bonds. This is the contrary of what observed with benzene, which tends to act as hydrogen bond donor towards anions and lone pair bearing

atoms alike. The *s*-tetrazine moiety instead seems to behave rather as hydrogen bond acceptor, a behaviour which is only possible with hydrogen bearing species, thus partially affecting lone pair contacts distribution (Figure 19) but not that of anions (Figure 21), generally lacking the proton (cf. discussion on the effect of the role of hydrogen bonding in lone pair distribution around arenes in section 4).

Another possible side note could be to not trust blindly our eyes: probability hotspots exists even at the periphery, especially for lone pairs (Figures 18 and 19), but they clearly do not correspond to any specific chemical interaction. Even with a thorough sampling, when projecting 3D data on a plane as a function of radius we tend to see a slight bias. Nevertheless, this is indicative of the relative strength of anion-π and lone-pair-π interactions with *s*-tetrazine. Lone pairs show a more or less random distribution beyond a certain distance from the centroid, while anion distribution is much more gathered even at higher offset values. This means that in the case of lone pair-π interactions either the interaction is weaker compared to the other supramolecular forces determining the exact position of each contact, or the interaction possesses a limited action range, if not both the above instances. Anion-π interactions, conversely, seems to be more intense, or possessing a longer reach, or both. These observations are once more perfectly in line with what is a priori expected for electrostatic and simply dipolar interaction types.

In conclusion, we have demonstrated how characteristic patterns exist for both oxygen anion and lone pair bearing atoms around the *s*-tetrazine ring. The characteristic probability hotspot patterns are indicative of the presence of anion-π and lone-pair-π forces which manifest a directional character. Directionality depends on the intrinsic properties of the considered heterocycle, with manifest connection to the ESP of the tetrazine molecule.

Lone pair-π interactions are found to be short range interactions of modest strength compared to the van der Waals and packing forces governing the overall contacts distributions around the *s*-tetrazine ring. Significant deviation in the hits distribution due to this kind of forces, although detected, pertains only to the area above the aromatic ring and the region in the immediate vicinity of the centroid (cf. Figure 19).

Proof of the existence of these contacts is of special importance, since it has previously been demonstrated through CSD survey of inappropriate quality and later disproved, repeating the study with unbiased queries [158], in the case of benzene. The present study points out that, provided the arene has a sufficiently high and positive quadrupolar moment, these dipole-quadrupole interactions, as modest as they can be, are indeed at work. This is also relevant due to the technical difficulties of accessing experimentally this kind of information, as lone pair-π interactions are problematic to evaluate in general, both owing to their strength, which is comparable to van der Waals contacts, and to the difficulty to observe these forces in isolation (i.e. without concomitant effects from other supramolecular forces, solvent effects, etc.).

Anion-π interactions are found to be much stronger, and capable, at least for the discussed case of *s*-tetrazine, of deeply affecting the overall contacts distribution even in a long-range manner. By this, we do not imply that such interactions possess an intrinsic long range, but that they are strong enough to cause a large percentage of hits to fall in the area amenable to the interaction, so that, examining data from a statistic viewpoint, everything else (i.e. contacts which are less dense of chemical sense) subside entirely (cf. Figure 21 and the lack of random scattering in probability hot-spots compared to Figure 19).

4. Selected evidences of anion-π and lone pair-π interactions with *s*-tetrazines in the solid state

Anion-π interaction are well established for what concerns the expected coordination geometry, with both electrostatic (charge-quadrupole) and polarization (charge-ring induced dipole) terms favouring the localization of the anion right above the centroid of the aromatic ring [11,105,159,160]. In this regard, *s*-tetrazine makes no exception.

The simplest and chiefly prototypical examples of this kind of interactions feature spherical halide anions, as they remove the influence of the anion's geometry on the spatial arrangement of the system. For what *s*-tetrazine is concerned, most of the evidence so far comes from a recent paper [73], where strong anion-π interactions were demonstrated in solution and in the solid state for 3,6-bis[(morpholin-4-yl)ethyl]-1,2,4,5-tetrazine with the whole series of halide anions.

As displayed in Figure 22, in all cases we observe short and centred contacts between the *s*-tetrazine moiety and the anions.

Figure 22 to be inserted about here

Other examples of halide anions complexes with various *s*-tetrazine-based ligands exist in the literature, all of them exhibiting geometries which are very close to the ideal one. If fluoride and bromide are not otherwise represented in the CSD beyond what displayed in Figure 22, examples of chloride and iodide complexes are reported. ROKBOK [161], tetraethylammonium 2,7,12,17,22,27-hexaoxa-4,5,14,15,24,25,33,34,37,38,41,42-dodecaazaheptacyclo[26.2.2.23,6.28,11.213,16.218,21.223,26]dotetraconta-1(30),3,5,8,10,13,15,18,20,23,25,28,31,33,35,37,39,41-octadecaene chloride, Figure 23, displays 3 non-symmetry related chloride anions, each of them forming at least one centred anion-π contact with the *s*-tetrazine rings belonging to the large macrocyclic molecule, while one of the anions is sandwiched between two distinct *s*-tetrazine moieties. Another wonderful example is provided by the Ni(II)-based scaffold of VAVSUH [125], tetrakis(m2-3,6-bis(2-Pyridyl)-1,2,4,5-tetrazine-N,N',N'',N''')-octakis(acetonitrile)-tetra-nickel(ii) iodide clathrate heptakis(hexafluoro-antimony), Figure 24, where a large symmetrical cage holds together 4 tetrazine subunits which form a perfect binding site for the large iodide anion, filling the space forming short (3.27 and 3.52 Å) and perfectly centred (offset = 0.0 Å in both cases) anion-π contacts.

Figures 23 and 24 to be inserted about here

As manifest from (Figure 6), also a minority of off-centred contacts exist with halogen atoms. These however, belong to interhalogen anions, with triiodide being the most common among them. One of the most impressive examples available of multiple anion-π contacts with polyhalogen anions is provided by the crystal structure VAVTES [125], tetrakis(m2-3,6-bis(2-Pyridyl)-1,2,4,5-tetrazine-N,N',N'',N''')-

(acetonitrile)-heptabromo-tetra-nickel(ii) tribromide clathrate acetonitrile toluene solvate, Figure 25, where a rather exotic tribromide anion is hosted within a large cage-like Ni(II) complex, forming multiple contacts with a total of 4 *s*-tetrazine rings. As one can immediately detect, the central bromine atom, which is formally the charge bearing one, is once more found in an almost perfectly centred position, i.e. once more observing the theoretically most stable interaction geometry. The adjacent bromine atoms, although contributing to the overall interaction, must then necessarily occupy off-centred sites. Incidentally, this provides an elegant way to introduce the problems connected with polyatomic anions and their polyhedral geometry.

Figure 25 to be inserted about here

The preference of halide anions for centred position over the aromatic ring and the fact that off-centred interactions are entirely due to linear interhalogen anions, are easy to ascertain trends due to the slim number of available crystal structures. This may not be the case for all polyatomic anions, which show further structural variety and have been shown to be able to adopt distinct interaction geometries depending on their shape.

Planar anions, among which trigonal ones (e.g. nitrate) are more commonly encountered, have long been known to prefer a flat disposition above the aromatic ring, as such an arrangement allows for better π-π-like interactions due to the planar geometry of the anion. A possible example of this classical arrangement is provided by stacked arrangements of tetrazine rings and nitrate anions in the crystal packing of the MOF-like structure LIWFEE [162], catena-[bis(3,6-di(pyridin-4-yl)-1,2,4,5-tetrazine)-dinitrato-cadmium(ii) tetrakis(thiourea)-cadmium(ii) dinitrate], displayed in Figure 26. However, the presence within a crystal structure of multiple contacts and forces, together with anion and ligand geometrical constraints, may cause considerable deviations from the expected interaction geometry up to the point of overriding it entirely. A perfect case in point is offered by the Cu(II) complex of SUPGAN [163], (nitrato)-bis(3-(3,5-dimethyl-1H-pyrazol-1-yl)-6-(3,3-dinitroazetidin-1-yl)-1,2,4,5-tetrazine)-copper nitrate acetonitrile solvate, Figure 27, where two distinct *s*-tetrazine rings are forced by the symmetry of the complex to lie on almost perpendicular planes (angle between mean ring planes 78.4°). Given the impossibility of a nitrate anion to form parallel anion-π interaction with both moieties, we found it giving a parallel interaction with the first one (angle between NO_3^- and *s*-tetrazine mean planes 8.7°) and a centred perpendicular (angle between NO_3^- and *s*-tetrazine mean planes 82.83°) anion-π interaction with the second one.

Figures 26 and 27 to be inserted about here.

Three-dimensional anions possess even more options. Examples of apical (one contact), lateral (2 contacts) and facial (3 contacts) anion-π interactions geometries featuring the tetrahedral perchlorate anion are displayed in Figure 28. This structural variety, depending on the surroundings of individual anions in each crystal lattice, becomes more complicated the more interacting sites the anion possesses. Overall it depends on the anion global symmetry (even relatively simple tetrahedral species may not possess Td symmetry, as is the case for thiosulphate) and on the nature of the *s*-tetrazine host itself, which may come with any type of substituents differing for symmetry, quadrupole moment, polarizability, steric hindrance and possibility to form other kinds of interaction with the anion, ultimately affecting its localization.

Figure 28 to be inserted about here.

These very reasons are the ones that prompted us to refrain from indicating quintessential examples showcasing the ideal interaction mode, selecting instead a few limit cases, pointing out the complexity of the issue, and to perform a statistical evaluation of all contacts between anions and *s*-tetrazine, as no case by case inspection could ever possibly provide a unique picture on the matter. Despite that, we should remember that complexity is not negative per se, sure it means difficulties, but it also comes with challenges and possibilities, eventually leading to accomplishment and beauty. Dunbar and co-workers reported a wonderful example of the anion templated self-assembly and interconversion of *s*-tetrazine-containing metallacyclophanes [125]. In their case, templating action of anions of different geometries led to the formation of molecular squares in the presence of tetrahedral, ClO_4^- (cf. VAVTAO, Figure 28) and BF_4^- (cf. relative discussion in section 5), and spherical, I^- (cf. VAVSUH, Figure 24) anions, molecular pentagons with the octahedral anion SbF_6^-, QEZVIA [125,165], Figure 29, and molecular triangles in the case of trigonal NO_3^- anion (indirectly observed through mass spectrometry but not isolated in crystalline form). To date this is one of the most striking examples of how deep understanding of relevant interaction patterns could translate into a valuable tool the intrinsic complexity of anion-π interaction with *s*-tetrazines.

Figure 29 to be inserted about here.

If possible, lone pair-π contacts revealed themselves as an even more thorny issue.

This type of interactions lies at the weak-side end of the spectrum of supramolecular forces. While it is true that anion-π interactions are not strong interactions either, lone-pair-π contacts can be thought of as having the same nature, but with dipolar contributions instead of charge ones. This means that the main stabilizing contribution (i.e. the electrostatic term) in a lone pair-π interaction will come from a dipole-ring quadrupole interaction, while polarization effects are expected to be extremely modest, as they become of the dipole- induced ring dipole type. Moreover, as for classical van der Waals forces, which are highly cooperative and whose contribution is undeniably present and effecting the overall stability and arrangements of crystalline phases, it is rather difficult to observe lone pair-π forces in isolation, which further complicates the ascertainment of the relevance and even of the existence of these forces.

When dealing with lone pair-π contacts in the CSD, previous reports [1,4], and even currently implemented fragments and ligands built in Isostar, are mainly focusing over small fragments (e.g. carbonyl C=O group, which might be attached to other functionalities of any kind) or small molecules (water and ammonia being highly prototypical). Figure 30 reports H_2O and C=O fragments distributions that may be generated for *s*-triazine using Isostar. While it is true that statistically many contacts are found among generic arenes and small molecules, especially solvent ones, which would support the use of arene-solvent molecules as valuable screening system for identifying lone pair-π interaction trends, it should also be considered that such small molecules may or may not occupy the observed position due to lone pair-π contacts alone, and, generally speaking, they will not. An insightful case in point is provided by the crystal structure NERQAE [166], catena-[(m4-5,5'-(1,2,4,5-Tetrazine-3,6-diyl)bis(tetrazolido))-tetrakis(m2-aqua)-di-sodium(i)

dihydrate]. It is totally possible to present in good faith the H_2O···*s*-tetrazine interaction displayed in Figure 31a (O…centroid 3.01 Å, offset 0.2 Å, angle 86.4°) as the paragon of strong and centred lone pair-π interactions, especially if the structure is selected using interaction parameters provided by a Conquest query and no further checked. Yet a detailed inspection (Figure 31b) would reveal said H_2O molecule to be involved in a hydrogen bond pattern with neighbouring metal coordinated water molecules and tetrazole nitrogen atoms. Thus, indicating single structures as examples of lone pair-π interactions should always be done carefully, while statistical analysis of aggregated results should be regarded as the most reliable method for identifying relevant interaction patterns whenever present. This is manifest in the comparisons of Figure 30a and Figure 30b: despite hydrogen bonding being the preponderant interaction mode for water, deeply affecting its distribution around *s*-triazine core (Figure 30b), a smaller but significant subset of data is still found creating a hit-dense region right above the ring centroid (Figure 30a), indicating a lone pair-π type interaction. According to these considerations, in the light of the fact that solvent molecules intrinsically tend to occupy voids in the crystal packing (if any) and generally present several possible binding modes beyond lone pair-π contacts (H-bonds, halogen bonds, etc.) it is best to look elsewhere for proper single examples of lone pair-π contacts, leaving contacts involving solvent molecules to statistical analysis instead.

Figures 30 and 31 to be inserted about here.

According to this reasoning we focused our attention on minimal crystal structures, featuring as few discrete species as possible (ideally one), with involved molecules not being expected to be able to resort to other interactions except van der Waals forces and, eventually, lone pair-π interactions.

A rather interesting collection of examples emerged.

The simple 3,6-bis[(morpholin-4-yl)methyl]-1,2,4,5-tetrazine molecule found in DETNAU [73] (Figure 32) organise itself in the crystal phase in such a way to bring the morpholine oxygen in close contact with the centroid of a neighbouring *s*-tetrazine moiety. Interaction parameters (O…centroid 2.96 Å, offset 0.15 Å, angle 86.9°) are indicative of a prototypical and strong interactions, as the oxygen atoms is found lying at a significantly shorter distance than the mere sum of (O+ring atom) vdW radii (about 7-10% shorter depending if O…N or O…C radii are used).

Figure 32 to be inserted about here.

The superior homologue 3,6-bis[(morpholin-4-yl)ethyl]-1,2,4,5-tetrazine in DETNEY [73] (Figure 33) showcases analogous short lone pair-π contacts: this time the nitrogen atom of the morpholine pendant being preferred. Once more, the interaction is strong (3.24 Å, 6-3% shorter than the sum of vdW radii, cf. above) and centred (offset 0.18 Å, angle 88.9°) resulting in the main detectable interaction imposing geometrical constraints within the crystal structure.

Figure 33 to be inserted about here.

Although these considerations could be further extended to superior propyl and butyl homologues, [75] giving weaker and weaker lone pair-π interactions as non-directional van der Waals contacts among longer and longer aliphatic pendants start to prevail, it is safer to look for examples elsewhere to provide a complete picture beyond the properties of a homologous molecules sampling pool.

The structure of the simple 3,6-bis(1-Aziridinyl)-1,2,4,5-tetrazine, FIZJIH (Figure 34) [167], and 1,2,4,5-tetrazine-3,6-dicarbonitrile, JOYXEC (Figure 35) [168], provide some valuable examples. The peculiarity of these structures is that they both contain very simple organic molecules constituted by the tetrazine core and decorated with N-containing pendants, thus are not expected to exhibit any peculiar supramolecular interaction beyond simple π-π stacking forces. Although FIZJIH may seem to display offset face to face π-π interactions, a close inspection (Figure 34) reveals that the overlap between neighbouring π clouds is almost non-existent, while strong (N…centroid 3.12 Å, offset 0.18 Å, angle 86,7°) "head to tail" lone pair-π interactions are found instead. Conversely, in the structure of JOYXEC (Figure 35) formation of π-π contacts between neighbouring *s*-tetrazine rings is not observed at all, the only short contacts (<ΣvdW radii) are those between the terminal N of the nitrile group and adjacent *s*-tetrazine, i.e. lone pair-π contacts. These forces, which according to experimental parameters are once more found strong and centred (N…centroid 2.83 Å, offset 0.20 Å, angle 85.94°), are manifestly strong enough to keep the crystal packing together.

Figures 34 and 35 to be inserted about here.

This seems to demonstrate that, granted the marked tendency of *s*-tetrazine to interact with electron rich species (cf. Figure 14), if no other stronger binding modes govern the reciprocal arrangement of these relatively simple molecules, there may be a tendency (and indeed there is from statistical analysis of the data, cf. Figures 17 and 19) of these systems to orient in such a way to have electron-rich, lone pair-bearing atoms (e.g. O, N) pointing right towards the centroid of a neighbouring *s*-tetrazine ring. The lack of directional supramolecular interactions (all most likely to be stronger than lone pair-π contacts in absolute terms) allows these forces to manifest themselves plainly (cf. Figures 32-35). As such, we believe to have provided statistical and structural evidence for the existence of these forces, their full recognition and potential role being paramount for future application in crystal engineering and discovery of potential drugs featuring the *s*-tetrazine ring as an active component.

5. Anion-π and lone pair-π interactions with *s*-tetrazines in solution

Solution studies on the formation of anion complexes involving interaction of *s*-tetrazines rings in solution are still rather rare. Earlier evidences were reported by Dunbar and co-workers, who discovered the unusual, high-yield formation of the cyclic square tetramer $[Ni_4(bptz)_4(CH_3CN)_8][BF_4]_8$ from solutions of $[Ni(CH_3CN)_6][BF_4]_2$ and bptz in methanol at room temperature [169]. The X-ray structure of the new compound revealed that one of the BF_4^- anions resides in the square cavity (Figure 36).

Drawing of ligand bptz to be inserted about here.

Figure 36 to be inserted about here.

An analysis of this structure shows that each fluorine atom of the included BF_4^- gives rise to a couple of anion-π interactions with one of the tetrazine rings, the shortest distances from the ring centroid being in the range 2.72-2.87 Å corresponding to offset values of 0.47-0.68 Å. The encapsulated anion appears to act as a template in the self-assembly process of the cyclic oligomer as evidenced by the fact that the formation of the square complex was not observed in the presence of other anions. Indeed, FAB mass spectrometric analysis of solutions of Ni ions with bptz in the presence of various anions indicated that only solutions containing the BF_4^- ion give a mass cluster corresponding to the square complex, in contrast to those containing PF_6^-, SbF_6^-, or $CF_3SO_3^-$.

Encouraged by these results, the same group launched a comprehensive investigation of the anion-templated self-assembling of similar oligomers, obtaining the formation of discrete molecular squares $[\{M_4(bptz)_4(CH_3CN)_8\}\subset X][X]_7$, (M = Ni, Fe, Zn; X^- = BF_4^-, ClO_4^-) and pentagons $[\{Ni_5(bptz)_5(CH_3CN)_{10}\}\subset SbF_6][SbF_6]_9$, $[Fe_5(bptz)_5(CH_3CN)_{10}][Y]_{10}$ (Y^-= SbF_6^-, AsF_6^-, PF_6^-), which were isolated in high yields [10]. In all cases, as shown by crystal structures, the central tetrazine ring of the ligand forms anion-π interactions with the encapsulated anions, which act as selective templating elements able to stabilize a particular metallacycle over another.

Electrospray ionization mass spectrometry, electrochemical, optical and NMR studies demonstrated the persistence of these oligomeric structures in solution, their stability being strictly dependent upon the inclusion of a specific anion. Complete conversion of an oligomer into a different one could be reversibly effected by adding an excess amount of the anion that stabilizes the other cavity size [125,165,170].

Selective binding and colorimetric sensing of F^- anions was achieved in DMSO solution by means of the metal-free macrocyclic amide ligand **1** containing an *s*-tetrazine ring [65]. The formation of F^- complex with **1** is denoted by a significant change of the absorption properties of the ligand in the UV and visible regions occurring upon the addition of F^-, the colour of the solution changing from red to green. Such a colour change was attributed to the formation of a tetrazine radical anion formed via an electron transfer process facilitated by anion-π (tetrazines–F^-) interaction within the complex. Indeed, DFT modelling of the [(**1**)F]$^-$ complex showed that, in the calculated structure, the fluoride anion lies in the cavity formed by the amide N–H groups and the tetrazine ring, giving rise to strong hydrogen bond and anion-π interactions. Similar calculations showed that the size of the ligand cavity is too small to host Cl^-, Br^- and I^- anions, thus preventing their interaction with the tetrazine ring. Accordingly, no significant changes were observed in the UV-vis spectra of **1** upon addition of these anions, as well as upon addition of other competitive anions such as N_3^-, PF_6^-, AcO^- and $H_2PO_4^-$. Furthermore, this sensing system is poorly affected by water, which is a strong inhibitor of fluoride sensors, tolerating up to 10% of water in DMSO.

Drawing of ligand **1** to be inserted about here.

Water is in general a problematic solvent to study the formation of anion complexes, owing to the strong and competitive solvation that anions suffer in this medium, but in the special case of tetrazines, the issue

is complicated by the low water solubility of these aromatic compounds. It was recently shown that solubilisation in water of tetrazine derivatives can be achieved by the formation of supramolecular inclusion compounds with β-cyclodextrin [171]. An alternative strategy, consisting in the functionalization of *s*-tetrazine with hydrophilic substituents on the carbon atoms, was adopted to enhance the water solubility of *s*-tetrazine, avoiding forcing the molecule into a confined environment and limit its capacity to interact with exogenous species. Insertion of aliphatic chains of different lengths bearing terminal morpholine groups provided the four **2**-**5** ligands endowed with sufficient solubility to be studied in water [71,75]. Protonation of the morpholine groups favours the solubility of these ligands and promotes their interaction with anions. A fair number of crystal structures of complexes of inorganic anions (halides, HF_2^-, I_3^-, SCN^-, NO_3^-, ClO_4^- and PF_6^-) with the diprotonated molecules H_2L^{2+} (L = **2**-**5**) showed that, despite their different geometries, the anions are invariably placed above the tetrazine rings, at short distance from their centroids [71-75]. Examples of anion complexes formed by H_2L^{2+} in the solid state are shown in Figure 37.

Drawing of ligands **2**-**5** to be inserted about here.

Figure 37 to be inserted about here.

These anion-π interactions are the distinctive elements of these crystal structures although they are commonly accompanied by other weak interactions (electrostatic, hydrogen bonds). The existence of such complexes in aqueous solution was proved by means of thermodynamic methods (potentiometric titrations, isothermal titration calorimetry (ITC)) and, in a special case [71], by pulsed gradient spin echo (PGSE) NMR diffusion spectroscopy. Speciation of the complex systems showed that anions interact with the protonated HL^+ and H_2L^{2+} and in several cases even with the free (unprotonated) L ligand species. A notable feature of these systems is that the stability constants of the complexes are poorly related to the ligand charge, indicating that their formation is not governed by the dominating charge-charge attraction that is normally observed in the formation of anion complexes with positively charged ligands [172], other forces must furnish the decisive contribution making favourable such association events. This observation, along with the surprising formation of stable anion complexes with free (not-protonated) ligands and the crystallographic evidences, supported the conviction that anion-π interactions make a prominent contribution to the stability of these anion complexes in water.

Free energy changes ($-\Delta G°$) in the range 10-17.5 kJ/mol were determined for the formation the anion complexes ($AL^{-/2-}$, $A^{-/2-}$ = NO_3^-, PF_6^-, ClO_4^-, and SO_4^{2-}; L = **2**, **3**) with the free L ligands [71]; values that well compare with the free energy changes ($-\Delta G°$ = 8.6-12 kJ/mol) previously determined for complexes, formed in water by inorganic anions with pyrimidine ligands, in which the anion-π interaction was thought to be the almost unique binding force [32,145].

Dissection of $\Delta G°$ values into their enthalpy ($\Delta H°$) and entropy ($T\Delta S°$) contributions, by means of ITC measurements, showed that the formation of these complexes is promoted by favourable entropic contributions, the associated enthalpy changes being very small, though favourable [71]. Such thermodynamic features were attribute to desolvation effects accompanying the pairing process, as desolvation is typically endothermic and exoentropic. Indeed, the occurrence of a significant desolvation occurring upon the formation of these complexes was confirmed by PGSE NMR diffusion spectroscopy that

led to the unprecedented observation that the charged (H_2(**3**)$^{2+}$) ligand undergoes a significant shrink in size (increase of diffusion coefficient) upon interaction with an anion (PF_6^-).

Interestingly, equilibrium data for the formation of anion complexes with **2** and **3** in a 80:20 (v:v) water:ethanol mixture, showed that a decrease of the dielectric constant of the medium (ε = 78.56 for pure water and ε = 69.05 for the mixture at 25°C) causes a general lowering of stability for complex with protonated ligand forms, while complexes of the unprotonated ligand become undetectable. Such observation was taken as a further evidence of the marginal role played by coulombic attraction in these association processes. As the presence of 20% of ethanol affect very little the solvation sphere of the anions, the loss of stability observed in the aqueous-ethanolic solution, relative to pure water, was ascribed to a stronger ligand solvation in the mixed solvent which appears particularly competitive with the formation of complexes with neutral ligands, that is with the formation of anion-π interactions [71].

A particular behaviour was exhibited by the halide complexes of **3**. As shown in Figure 38, the equilibrium constants (*K*) for the complexation reactions H_2(**3**)$^{2+}$ + X^- = [H_2(**3**)X]$^+$ (X = F, Cl, Br, I) give rise to a V-shaped profile with a minimum for Cl^-, in contrast with crystallographic results showing stronger association of Cl^- and Br^- with H_2(**3**)$^{2+}$ via simultaneous anion-π and salt-bridge interactions in the solid state. This behaviour was rationalized by considering the combination of opposite trends: *i*) contributions becoming weaker along the F^-–I^- series (charge density of the anions, ability to form H-bonds, polarization of the ligand π-electron system induced by the anions, all suggesting a steady weakening of both anion-π and salt-bridge contributions), *ii*) energetic cost for anions' desolvation decreasing in the order $F^- > Cl^- > Br^- > I^-$ ($\Delta G°_{hyd}$ -472 kJ/mol (F^-), -347 kJ/mol (Cl^-), -321 kJ/mol (Br^-), -283 kJ/mol (I^-)) that favours complexation in the opposite direction.

Figure 38 to be inserted about here.

A remarkable feature of L1-L4 is their ability to bind OH^- in water when they are in the form of unprotonated amines, a finding which was unprecedented for organic receptors in water. Such [(L)OH]$^-$ (L = **2**-**5**) species are the most stable complexes (in the case of **4** and **5**) or among the most stable complexes (in the case of **2** and **3**) formed by **2**-**5** with inorganic anions [71-75].

The free energy changes ($\Delta G°$) associated to the formation of these complexes ($\Delta G°$ from -10.0 to -15.3 kJ/mol) suggested that both anion-π interactions and hydrogen bonding of OH^- with the nitrogen atoms of the morpholine ligand residues contribute to complex stability. While $\Delta G°$ of complexation did not show a particular trend for these hydroxo-complexes [(L)OH]$^-$ (L = **2**-**5**), the associated enthalpy contributions ($\Delta H°$), measured by ITC, turned out to be considerably less exothermic (less favourable) for **4** and **5** than for **2** and **3**, whereas the entropic ones ($T\Delta S°$), that were unfavourable (negative) for **2** and **3**, became favourable (positive) for **4** and **5**. Such behaviour might be indicative of a lower (or absent) participation of the ligand chains in stabilizing the OH^- complexes via hydrogen bonding, that is, the associated favourable enthalpic contribution for hydrogen bonding would be lost, while a favourable entropic contribution would be gained for the increased freedom of the not-coordinated ligand chains [71,73].

Despite, in several cases, anion-π interactions seem to be the dominating forces in determining the stability of the complexes of tetrazine-based ligands with anions, no models are available to date for isolated anion-π contacts with tetrazines.

This is very close to being a general reality, at least by now, for this type of non-covalent interaction that emerges, to a greater or lesser extent, from the interplay of various weak forces. When organic anions are considered, instead of inorganic ones, the picture becomes more complicate, as further interactions, such as π-stacking, and solvation phenomena, like the hydrophobic effect, can participate to the association processes, while the stereochemistry of the interacting groups and the host-guest mutual size introduce additional variables. To further complicate the matter, most of organic anions are conjugate bases of weak acids, that is, protonation may extinguish the negative charge of anions and anionic forms may exist in narrow pH windows.

Within this frame, the interaction of **2** and **3** with $CH_3SO_3^-$, CH_3COO^-, $C_6H_5SO_3^-$, $C_2H_5COO^-$, phthalate (Pth^{2-}) and isophthalate ($IPth^{2-}$) was investigated by means of thermodynamic, NMR and XRD methods as well as by in silico simulations [76]. The results evidenced that geometrical features and size/shape complementarity of anions and ligands are the most important factors in orchestrating the interplay of supramolecular forces that stabilize these complexes, giving rise, with the help of solvation effects, to remarkable features of binding selectivity. Indeed, for the series of monoanionic species, both 2 and 3 complexes show a stability trend which follows the orders: *i*) benzoate ≥ acetate > benzenesulfonate > methanesulfonate, i.e. carboxylate > sulfonate and *ii*) aromatic > aliphatic. Moreover, **2** forms more stable complexes with isophthalate than with phthalate, while the contrary is true for **3**. Instead, if we examine the data in terms of the affinity of the same anion for the two receptors, we find that both phthalate and isophthalate prefer **2** to **3** over a large pH range. Despite the number of forces involved, anion-π interactions were found to play an important role in the formation of these complexes. Whether intrinsically chosen by the systems or favoured by the disposition of ligands' hydrogen bond donors, they are preferred over π-stacking forces in most cases [76].

An analysis of solid state data for the complexes formed by **2**-**5** with both inorganic and organic anions [71-76], as well as for the crystal structures of the free ligands [73,75] shows that these molecules can fundamentally give rise to the six binding modes outlined in Scheme 3, while equilibrium and computational data seem indicative of the existence of similar interactions also in solution.

Scheme 3 to be inserted about here.

Anion-π interactions (type a) are rarely isolated, they are commonly found associated to long-range electrostatic attractions (type b), salt bridges (type c) and hydrogen bonds (type d). Binding modes of types a-d are generally formed by anions whose basicity is lower than the basicity of the morpholine groups and occur at pH near or below the pK_a of the morpholine groups. Indeed, they have been observed in many crystal structures of complexes of inorganic anions with protonated forms of **2**-**5** [71-75] and in H_2(**3**)(Hisophthalate)$_2$ [76]. c-d are the binding modes contributing most to the formation of complexes of inorganic anions with protonated ligands in solution, while type a, pure anion-π interactions, are the main responsible for the association between anions and neutral ligands. Similar to type a are type e interactions, since they do not involve the basic centres (the morpholine groups) of the ligands. They were found in the free ligands structures [73,75]. The interactions of type f, namely lone pair-π interactions

assisted by hydrogen bonds, have never been observed in crystal structures with **2**-**5**, although modelling calculations have shown that this binding mode should occur in the water adducts of **2** and **3** and their occurrence in solution might contribute to define the basicity properties of **2**-**5** and the stability of their hydroxo complexes [71].

Very recently, macrocyclic tetrahomocorona[2]arene[2]tetrazines **6**-**9** containing two faced *s*-tetrazine rings were constructed by coupling 3,6-dichlorotetrazine with *o*-, *m*-, and *p*-bis(hydroxymethyl)benzenes [173]. Quenching of ligand fluorescence was observed in acetonitrile upon titration with linear N_3^- and SCN^- anions, while the intensity of the emission bands of **6**-**9** remained almost intact even when very large amounts of differently shaped anions (Cl^-, NO_3^-, BF_4^-, PF_6^-) were added. Despite the host-guess complexation was not strong, the complex stability constants determined from fluorimetric titrations showed a binding preference for azide over thiocyanate and a greater binding ability of **6**, relative to **7**-**9**, toward both linear anions. According to computational analysis (B3LYP and 6-31 + G(d,p) basis set) of complex structures, in the most stable complex $[(\mathbf{6})N_3]^-$ the linear anion is chelated, via anion-π interactions within the ligand cavity, by two tetrazine rings, the terminal nitrogen atoms of the anion being located 2.88 Å and 3.09 Å, respectively, from the ring centroids (Figure 39a). The thiocyanate $[(\mathbf{6})SCN]^-$ complex displays a quite similar calculated structure, but the interaction of the sulfur atom with the tetrazine rings is weaker (3.53 Å) in agreement with the lower stability of the complex in solution. Calculated structures for the complexes with **7**-**9** showed a half-sandwich-type complexation with one nitrogen atoms of both azide and thiocyanate anions inserted into the ligand cavity (Figure 39b), the distance from the tetrazine rings ranging from 2.96 Å to 3.24 Å [173]. It is interesting to note that the size of macrocycles and the topology of the binding sites (the tetrazine rings) provide effective criteria for anion binding selectivity.

Drawing of ligands **6**-**9** to be inserted about here.

Figure 39 to be inserted here.

In conclusion, despite the fact that the thermodynamic data for the formation of anion-π interactions by *s*-tetrazines in solution are still few in number and, for the most part, they cannot be easily isolated and extracted from the interplay of weak forces that characterize the host-guest chemistry of anions, the body of information reported in this section, though limited, appears as a prelude to a future greater spread of tetrazine rings within the library of building blocks available for design and construction of receptors for effective anion binding and recognition in solution.

6. Conclusions

The manifest objective of this study was establishing the usage of *s*-tetrazines in anion receptors by providing substantial experimental grounds of their usefulness as binding sites for anions, both in solution and in the solid state. On a more fundamental level, it offered us the possibility to extend the investigation to lone pair-π interactions, expanding the limited amount of literature dedicated to interactions falling within the weakest part of the spectrum of supramolecular forces.

The first section has been dedicated to exploring the fundamental properties of the *s*-tetrazine ring, making it considerably amenable to anion- and lone pair-π contacts, and to providing guidance on current synthetic approaches for the preparation and introduction of this heterocycle within larger receptors.

Then, examination of CSD data, both on qualitative and quantitative grounds (i.e. by inspecting both selected examples and global analysis of contacts), revealed characteristic probability hotspot patterns in the localization of both anion and lone pairs around the *s*-tetrazine nucleus. These are indicative of the presence of anion-π and lone-pair-π forces which manifest a directional character, directionality being dependent on the intrinsic properties of the considered heterocycle: in particular, manifest connection to the ESP of the tetrazine molecule has been observed. This trait has also been shown to match what could be anticipated on the basis of literature in silico simulations.

Lone pair-π interactions are found to be short range interactions whose strength is modest compared to van der Waals and packing forces governing the overall contacts distributions around the *s*-tetrazine ring. Significant deviation in the contacts distribution due to this kind of forces, although detected, pertains only to the immediate vicinity of the ring centroid. Detection alone could already be considered a valuable result in itself, especially considering the debate on the existence of these type of contacts and the technical difficulties connected to their evaluation. As we tried to show within the selection of discussed crystal structures, these forces tend to emerge manifestly especially in the case of simple molecules, which cannot rely on other, stronger, directional supramolecular forces. In those cases, a tendency to assume a mutual orientation maximizing lone pair-π contacts can be observed, leading to the understanding that, under the right circumstances, lone pair-π interactions might prove useful for crystal engineering purposes.

Conversely, anion-π interactions are found to be much stronger, and capable of deeply affecting the overall contacts distribution around the *s*-tetrazine nucleus. From a statistical standpoint, we can see that the effect appears to be quite long range, in the sense that it is able to confine the vast majority of the contacts along the C-C molecular axis and to polarize the whole contacts distribution towards the ring centroid. This appears to indicate anion-π both as a rather frequent, and thus arguably a rather intense, interaction type for *s*-tetrazines in the solid state.

The directionality observed in the solid state could be better exploited if *s*-tetrazine, a non-naturally occurring heterocycle, would be included into libraries of compounds intended for drug design and crystal engineering like Isostar, allowing for the evidences herein collected to be promptly and effectively put in practice.

The last section, dedicated to anion- and lone pair-π interactions with *s*-tetrazine-based ligands in solution, gathers the most relevant results reported so far. This provides literature grounds for the claim that the amenability of *s*-tetrazines to these types of interactions, which we demonstrated in the solid state, is nevertheless preserved to some extent also in solution. As such we believe that this last section of our study can be seen as a starting point and source of inspiration for a new generation of *s*-tetrazine solution receptors for electron-rich species.

Appendix A. Supplementary data

Supplementary data to this article can be found online at

References

[1] M. Egli, S. Sarkhel, Acc. Chem. Res. 40 (2007) 197–205.

[2] S. Sarkhel, A. Rich, M. Egli, J. Am. Chem. Soc. 125 (2003) 8998–8999.

[3] A. Bauzá, T.J. Mooibroek, A. Frontera, ChemPhysChem. 16 (2015) 2496–2517.

[4] A. Jain, V. Ramanathan, R. Sankararamakrishnan, Protein Sci. 18 (2009) 595–605

[5] Z. Lu, P. Gamez, I. Mutikainen, U. Turpeinen, J. Reedijk, Cryst. Growth Des. 7 (2007) 1669–1671.

[6] N. Hayashi, H. Higuchi, K. Ninomiya, Top. Heterocycl. Chem. 18 (2009) 1-35.

[7] T. J. Mooibroek, P. Gamez, J. Reedijk, CrystEngComm 10 (2008) 1501-1515.

[8] D. Quiñonero, A. Frontera, P. M. Deyà, Anion-π Interactions in Molecular Recognition, in Anion Coordination Chemistry; K. Bowman-James, A. Bianchi, E. García-España, Eds., Wiley-VCH, New York, 2012.

[9] K. Xiaonan, L. Hui, P. Qingyan, L. Zhibo, Z. Yingjie, Chin. Chem. Lett. 29 (2018) 261-266.

[10] H. T. Chifotides, K. R. Dunbar, Acc. Chem. Res. 46 (2013) 894–906.

[11] A. Frontera, P. Gamez, M. Mascal, T.J. Mooibroek, J. Reedijk, Angew. Chem. Int. Ed. 50 (2011) 9564–9583.

[12] I. Alkorta, F. Blanco, P. Deyà, J. Elguero, C. Estarellas, A. Frontera, D. Quiñonero, Theor. Chem. Acc. 126 (2010) 1–14.

[13] H.–J. Schneider, Angew. Chem., Int. Ed. 48 (2009) 3924–3977.

[14] O. B. Berryman, D. W. Johnson, Chem. Comm. (2009) 3143-3153.

[15] B. L. Schottel, H. T. Chifotides, K. R. Dunbar, Chem. Soc. Rev. 37 (2008) 68–83.

[16] D. Quiñonero, C. Garau, C. Rotger, A. Frontera, P. Ballester, A. Costa, P.M. Deyà, P.M. Deya, Angew. Chem. Int. Ed. 41 (2002) 3389–3392.

[17] M. Mascal, A. Armstrong, A.; M. D. Bartberger, J. Am. Chem. Soc. 124 (2002) 6274–6276.

[18] I. Alkorta, I. Rozas, J. Elguero, J. Am. Chem. Soc. 124 (2002) 8593–8598.

[19] K. Hiraoka, S. Mizuse, S. Yamabe, J. Phys. Chem. 91 (1987) 5294–5297.

[20] J. W. Steed, J: Atwood, Supramolecular Chemistry, 2nd ed., John Wiley & Sons, Chichester,2009.

[21] E. R. T. Tiekink, Crystal Engineering, in Supramolecular Chemistry: From Molecules to Nanomaterials, P. A. Gale, J. W. Steed, Eds., John Wiley & Sons, Chichester, 2012.

[22] J. Kozelka, Eur. Biophys. J., 46 (2017) 729-737.

[23] S. Chakravarty, A. R. Ung, B. Moore, J. Shore, M. Alshamrani, Biochem. 57 (2018) 1852-1867.

[24] M.S. Smith, E.E.K. Lawrence, W.M. Billings, K.S. Larsen, N.A. Bécar, J.L. Price, ACS Chem. Biol. 12 (2017) 2535–2537.

[25] M. Giese, M. Albrecht, K. Rissanen, Chem. Commun. 52 (2016) 1778–1795.

[26] X. Lucas, A. Bauza, A. Frontera, D. Quinonero, Chem. Sci. 7 (2016) 1038–1050.

[27] U., Rewati Raman, P. Debashis. S. Anand Pratap, K. Anuj, O. Umaprasana, K. Kumar, ACS Applied Nano Materials 1 (2018) 82-93.

[28] J. Yan, C. Kang, Z. Bian, X. Ma, R. Jin, Z. Du, L. Gao, Chem. Eur. J. 23 (2017) 5824–5829.

[29] N. Nassirinia, S. Amani, S. J. Teat, O. Roubeau, P. Gamez, Chem. Commun. 50 (2014) 1003–1005.

[30] Z. Aliakbar Tehrani, K. S. Kim, Int. J. Quantum Chem. 116 (2016) 622–633.

[31] J.-Z. Liao, H.-L. Zhang, S.-S. Wang, J.-P. Yong, X.-Y. Wu, R. Yu, C.-Z. Lu, Inorg. Chem. 54 (2015) 4345–4350.

[32] M. Savastano, P. Arranz-Mascarós, C. Bazzicalupi, A. Bianchi, C. Giorgi, M. L. Godino-Salido, M. D. Gutiérrez-Valero, R. López-Garzón, RSC Adv. 4 (2014) 58505–58513.

[33] R. Berger, G. Resnati, P. Metrangolo, E. Weber, J. Hulliger, Chem. Soc. Rev. 40 (2011) 3496-3508.

[34] P. Arranz, A. Bianchi, R. Cuesta, C. Giorgi, M. L. Godino, M. D. Gutierrez, R. Lopez, A. Santiago, Inorg. Chem. 49 (2010) 9321–9332; Inorg. Chem. 51 (2012) 4883.

[35] P. Molina, F. Zapata, A. Caballero, Chem. Rev. 117 (2017) 9907-9972.

[36] P. A. Gale, C. Caltagirone, Chem. Soc. Rev. 44 (2015) 4212–4227.

[37] N. H. Evans, P. D. Beer, Angew. Chem. Int. Ed. 53 (2014) 11716–11754

[38] M. Neetha; S. H. Cherumuttathu, J. Phys. Chem. A 118 (2014) 4315-4324.

[39] D.-X. Wang, Q.-Y. Zheng, Q.-Q. Wang, M.-X. Wang, Chem., Int. Ed. 47 (2008) 7485-7488.

[40] J. Kobylarczyk, D. Pinkowicz, M. Srebro-Hooper, J. Hooper, R. Podgajny, Cryst. Growth Des. 19 (2019) 1215-1225.

[41] J. Luo, Y.-F. Ao, C. Malm, J. Hunger, Q.-Q. Wang, D.-X. Wang, Dalton Trans. 47 (2018) 7883-7887.

[42] Y.-Z. Liu, K. Yuan, L. Liu, Z.Yuan, Y.-C. Zhu, J. Phys. Chem. A 121 (2017) 892-900.

[43] P. Hoog, A. Robertazzi, I. Mutikainen, U. Turpeinen, P. Gamez, J. Reedijk, Eur. J. Inorg. Chem. 18 (2009) 2684-2690

[44] L.M. Lee,M. Tsemperouli, A.I. Poblador-Bahamonde, S. Benz, N. Sakai, K. Sugihara, S. Matile, J. Am. Chem. Soc. 141 (2019) 810-814.

[45] M. Macchione, M. Tsemperouli, A. Goujon, A.R. Mallia, N. Sakai, K. Sugihara, S. Matile, Helv. Chim. Acta 101 (2018) e1800014.

[46] P. A. Gale, J. T. Davis R. Quesada, Chem. Soc. Rev. 46 (2017) 2497-2519.

[47] A. Vargas Jentzsch, S. Matile, Top. Curr. Chem. 358 (2015) 205–239.

[48] A. Vargas Jentzsch, A. Hennig, J. Mareda, S. Matile, Acc. Chem. Res. 46 (2013) 2791–2800

[49] A. V. Jentzsch, D. Emery, J. Mareda, S. K. Nayak, P. Metrangolo, G. Resnati, N. Sakai, S. Matile, Nat. Commun. 3 (2012) 905.

[50] A. Vargas Jentzsch, D. Emery, J. Mareda, P. Metrangolo, G. Resnati, S. Matile, Angew. Chem. Int. Ed. 50 (2011) 11675–11678.

[51] Y. Zhao, Y. Cotelle, L. Liu, J. López-Andarias, A.-B. Bornhof, M. Akamatsu, N. Sakai, S. Matile, Acc. Chem. Res. 51 (2018) 2255–2263.

[52] X. Zhang, X. Hao, L. Liu, A.-T. Pham, J. Lopez-Andarias, A. Frontera, N. Sakai, S. Matile, J. Am. Chem. Soc. 140 (2018) 17867-17871.

[53] Y. Aramaki, Yuki Gosei Kagaku Kyokaishi 75 (2017) 965-966.

[54] M. Breugst, D. Von der Heiden, J. Schmauck, Synthesis 49 (2017) 3224–3236.

[55] T. Lu, S. E. Wheeler, Org. Lett. 16 (2014) 3268–3271.

[56] Q.-Q. Wang, N. Luo, X.-D. Wang, Y.-F. Ao, Y.-F. Chen, J.-M. Liu, C.-Y. Su, D.-X. Wang, M.-X. Wang, J. Am. Chem. Soc. 139 (2017) 635-638.

[57] Y. Zhao, Y. Domoto, E. Orentas, C. Beuchat, D. Emery, J. Mareda, N. Sakai, S. Matile, Angew. Chem., Int. Ed. 52 (2013) 9940−9943.

[58] G. Men, W. Han, C. Chen,C. Liang, S. Jiang, Analyst 144 (2019) 2226-2230.

[59] P. A. Gale, C. Caltagirone, Coord. Chem. Rev. 354 (2018) 2-27.

[60] L.-L. Wang, H. Zhou, T.-L. Yang, H. Ke, Y.-K. Tu, H. Yao, W. Jiang, Chem. Eur. J. 24 (2018) 16757-16761.

[61] P.-Y. Gu, Z. Wang, Q. Zhang, J. Mat. Chem. B 4 (2016) 7060-7074.

[62] L. E. Solis-Delgado, A. Ochoa-Teran, A. K. Yatsimirsky, G. Pina-Luis, Anal. Lett. 49 (2016) 2301–2311.

[63] X. Fang, M.-D. Guo, L.-J. Weng, Y. Chen, M.-L. Lin, Dyes Pigm. 113 (2015) 251−256.

[64] C. Stephenson, K.D. Shimizu, Org. Biomol. Chem. 8 (2010) 1027-1032.

[65] Y. Zhao, Y. Li, Z. Qin, R. Jiang, H. Liu, Y. Li, Dalt. Trans. 41 (2012) 13338-13342.

[66] S. Guha, S. Saha, J. Am. Chem. Soc. 132 (2010) 17674–17677.

[67] C. Garau, A. Frontera, D. Quiñonero, P. Ballester, A. Costa, P.M. Deyà, ChemPhysChem. 4 (2003) 1344–1348.

[68] D. Y. Kim, N. J. Singh, J. W. Lee, K. S. Kim, J. Chem. Theory Comput. 4 (2008) 1162–1169.

[69] D. Y. Kim, N. J. Singh, K. S. Kim, J. Chem. Theory Comput. 4 (2008) 1401–1407.

[70] D. Kim, D.; E. C. Lee, K. S. Kim, P. Tarakeshwar, J. Phys. Chem. A 111 (2007) 7980−7986

[71] M. Savastano, C. Bazzicalupi, C. Giorgi, C. García-Gallarín, M.D. López de la Torre, F. Pichierri, A. Bianchi, M. Melguizo, Inorg. Chem. 55 (2016) 8013–8024.

[72] M. Savastano, C. Bazzicalupi, C. García, M. D. López de la Torre, P. Mariani, F. Pichierri, A. Bianchi, M. Melguizo, Dalton Trans., 46 (2017) 4518–4529.

[73] M. Savastano, C. Bazzicalupi, C. García-Gallarín, C. Giorgi, M.D. López De La Torre, F. Pichierri, A. Bianchi, M. Melguizo, Dalt. Trans. 47 (2018) 3329–3338.

[74] M. Savastano, C. García, M. D. López de la Torre, F. Pichierri, C. Bazzicalupi, A. Bianchi, M. Melguizo, M. Inorg. Chim. Acta, 470 (2018) 133-138.

[75] M. Savastano, C. Bazzicalupi, C. García-Gallarín, C. Giorgi, M.D. López de la Torre, A. Bianchi, M. Melguizo, submitted.

[76] M. Savastano, C. Bazzicalupi, C. García-Gallarín, M. D. López de la Torre, A. Bianchi, M. Melguizo, Org. Chem. Front. 6 (2019) 75–86.

[77] M. Savastano, C. Bazzicalupi, P. Mariani, A. Bianchi, Molecules 23 (2018) 572.

[78] A. Pinner, A. Salomon, Gobel. Berichte Der Dtsch. Chem. Gesellschaft. 30 (1897) 1871–1890.

[79] A. Pinner, Ber. Dtsch. Chem. Ges. 30 (1897) 1871–1890.

[80] A. Pinner, F. Klein, Berichte Der Dtsch. Chem. Gesellschaft. 10 (1877) 1889–1897.

[81] G. Clavier, P. Audebert, Chem. Rev. 110 (2010) 3299–3314.

[82] N. Saracoglu, Tetrahedron. 63 (2007) 4199–4236.

[83] P. Audebert, G. Clavier, C. Allain, Chapter 6.3 - Triazines, Tetrazines, and Fused Ring Polyaza Systems, in: G.W. Gribble, J.A.B.T.-P. in H.C. Joule (Eds.), Prog. Heterocycl. Chem.

Vol. 29, Elsevier, 2017: pp. 483–518.

[84] H. Wu, N.K. Devaraj, Acc. Chem. Res. 51 (2018) 1249–1259.

[85] A.J. Calahorro, B. Fernández, C. García-Gallarín, M. Melguizo, D. Fairen-Jimenez, G. Zaragoza, A. Salinas-Castillo, S. Gómez-Ruiz, A. Rodríguez-Diéguez, New J. Chem. 39 (2015) 6453–6458.

[86] M. Moral, G. García, A. Peñas, A. Garzón, J.M. Granadino-Roldán, M. Melguizo, M. Fernández-Gómez, Chem. Phys. 408 (2012) 17–27.

[87] W. Mao, W. Shi, J. Li, D. Su, X. Wang, L. Zhang, L. Pan, X. Wu, H. Wu, Angew. Chem. Int. Ed. 58 (2019) 1106–1109.

[88] M. Moral, G. García, A. Garzón, J.M. Granadino-Roldán, M.A. Fox, D.S. Yufit, A. Peñas, M. Melguizo, M. Fernández-Gómez, J. Phys. Chem. C. 118 (2014) 26427–26439.

[89] A.J. Calahorro, A. Peñas-Sanjuan, M. Melguizo, D. Fairen-Jimenez, G. Zaragoza, B. Fernández, A. Salinas-Castillo, A. Rodríguez-Diéguez, Inorg. Chem. 52 (2013) 546–548.

[90] Z. Fang, W.-L. Hu, D.-Y. Liu, C.-Y. Yu, X.-G. Hu, Green Chem. 19 (2017) 1299–1302.

[91] Y. Qu, F.X. Sauvage, G. Clavier, F. Miomandre, P. Audebert, Angew. Chem., Int. Ed. 57 (2018) 12057–12061.

[92] M.A. Hiskey, M.C. Johnson, D.E. Chavez, J. Energ. Mater. 17 (1999) 233–252.

[93] Q. Zhou, P. Audebert, G. Clavier, F. Miomandre, J. Tang, RSC Adv. 4 (2014) 7193–7195.

[94] E. Jullien-Macchi, V. Alain-Rizzo, C. Allain, C. Dumas-Verdes, P. Audebert, RSC Adv. 4 (2014) 34127–34133.

[95] S.G. Tolshchina, G.L. Rusinov, V.N. Charushin, Chem. Heterocycl. Compd. 49 (2013) 66–91.

[96] A.M. Bender, T.C. Chopko, T.M. Bridges, C.W. Lindsley, Org. Lett. 19 (2017) 5693–5696.

[97] C. Quinton, V. Alain-Rizzo, C. Dumas-Verdes, G. Clavier, L. Vignau, P. Audebert, New J. Chem. 39 (2015) 9700–9713.

[98] H. Wei, H. Gao, J.M. Shreeve, Chem. Eur. J. 20 (2014) 16943–16952.

[99] D.E. Chavez, D.A. Parrish, L. Mitchell, G.H. Imler, Angew. Chem. Int. Ed. 56 (2017) 3575–3578.

[100] S.E. Wheeler, J.W.G. Bloom, Chem. Commun. 50 (2014) 11118–11121.

[101] Y. Li, F. Miomandre, G. Clavier, L. Galmiche, V. Alain-Rizzo, P. Audebert, ChemElectroChem. 4 (2017) 430–435.

[102] C. Li, H. Ge, B. Yin, M. She, P. Liu, X. Li, J. Li, RSC Adv. 5 (2015) 12277–12286.

[103] F. Pop, J. Ding, L.M.L. Daku, A. Hauser, N. Avarvari, RSC Adv. 3 (2013) 3218–3221.

[104] M. Plugge, V. Alain-Rizzo, P. Audebert, A.M. Brouwer, J. Photochem. Photobiol. A Chem. 234 (2012) 12–20.

[105] C. Garau, D. Quiñonero, A. Frontera, A. Costa, P. Ballester, P.M. Deyà, Chem. Phys. Lett. 370 (2003) 7–13.

[106] K.D. Nanda, A.I. Krylov, J. Chem. Phys. 145 (2016) 204116.

[107] F. Pop, N. Avarvari, Chem. Commun. 52 (2016) 7906–7927.

[108] L. Guerret-Legras, P. Audebert, J.-F. Audibert, C. Niebel, T. Jarrosson, F. Serein-Spirau, J.-P. Lère-Porte, J. Electroanal. Chem. 840 (2019) 60–66.

[109] C. Wang, C. Li, S. Wen, P. Ma, G. Wang, C. Wang, H. Li, L. Shen, W. Guo, S. Ruan, ACS Sustain. Chem. Eng. 5 (2017) 8684–8692.

[110] P. Ma, C. Wang, S. Wen, L. Wang, L. Shen, W. Guo, S. Ruan, Sol. Energy Mater. Sol. Cells. 155 (2016) 30–37.

[111] J. Sun, Y. Chen, Z. Liang, Adv. Funct. Mater. 26 (2016) 2783–2799.

[112] H. Al-Kutubi, H.R. Zafarani, L. Rassaei, K. Mathwig, Eur. Polym. J. 83 (2016) 478–498.

[113] S. Seo, H. Shin, C. Park, H. Lim, E. Kim, Macromol. Res. 21 (2013) 284–289.

[114] S. Samanta, S. Das, P. Biswas, J. Org. Chem. 78 (2013) 11184–11193.

[115] D.J. Min, F. Miomandre, P. Audebert, J.E. Kwon, S.Y. Park, ChemSusChem. 12 (2019) 503–510.

[116] T. Zhang, J. Du, Z. Li, X. Lin, L. Wang, L. Yang, T. Zhang, CrystEngComm. 21 (2019) 765–772.

[117] Y. Qu, S.P. Babailov, J. Mater. Chem. A. 6 (2018) 1915–1940.

[118] J. Lavoie, C.-F. Petre, S. Durand, C. Dubois, J. Hazard. Mater. 363 (2019) 457–463.

[119] G. Wang, T. Lu, G. Fan, H. Yin, F.-X. Chen, New J. Chem. 43 (2019) 1663–1666.

[120] Y. Liu, G. Zhao, Y. Tang, J. Zhang, L. Hu, G.H. Imler, D.A. Parrish, J.M. Shreeve, J. Mater. Chem. A. 7 (2019) 7875–7884.

[121] H. Wu, N.K. Devaraj, Top. Curr. Chem. 374 (2016) 1–22.

[122] H. Zhu, H. Wu, M. Wu, Q. Gong, Curr. Org. Chem. 20 (2016) 1756–1767.

[123] A.M. Prokhorov, D.N. Kozhevnikov, Chem. Heterocycl. Compd. 48 (2012) 1153–1176.

[124] S. Mayer, K. Lang, Synth. 49 (2017) 830–848.

[125] C.S. Campos-Fernández, B.L. Schottel, H.T. Chifotides, J.K. Bera, J. Bacsa, J.M. Koomen, D.H. Russell, K.R. Dunbar, J. Am. Chem. Soc. 127 (2005) 12909–12923.

[126] B.L. Schottel, H.T. Chifotides, M. Shatruk, A. Chouai, L.M. Pérez, J. Bacsa, K.R. Dunbar, J. Am. Chem. Soc. 128 (2006) 5895–5912.

[127] A.J. Neel, M.J. Hilton, M.S. Sigman, F.D. Toste, Nature. 543 (2017) 637–646.

[128] A. Bauzá, D. Quiñonero, P.M. Deyà, A. Frontera, Chem. Phys. Lett. 567 (2013) 60–65.

[129] B.L. Schottel, J. Bacsa, K.R. Dunbar, Chem. Commun. (2005) 46–47.

[130] I.A. Gural'skiy, D. Escudero, A. Frontera, P. V Solntsev, E.B. Rusanov, A.N. Chernega, H. Krautscheid, K. V Domasevitch, Dalt. Trans. (2009) 2856–2864.

[131] C.S. Anstöter, J.P. Rogers, J.R.R. Verlet, J. Am. Chem. Soc. 141 (2019) 6132–6135.

[132] H. Wang, W. Wang, W.J. Jin, Chem. Rev. 116 (2016) 5072–5104.

[133] Y.P. Yurenko, S. Bazzi, R. Marek, J. Kozelka, Chem. Eur. J. 23 (2017) 3246–3250.

[134] A. Frontera, D. Quiñonero, P.M. Deyà, Cation–π and anion–π interactions, WIREs Comput. Mol. Sci. 1 (2011) 440–459.

[135] J.H. Williams, Acc. Chem. Res. 26 (1993) 593–598.

[136] D. Kim, P. Tarakeshwar, K.S. Kim, J. Phys. Chem. A. 108 (2004) 1250–1258.

[137] J.P. Wagner, P.R. Schreiner, Angew. Chem. Int. Ed. 54 (2015) 12274–12296.

[138] J. López-Andarias, A. Bauzá, N. Sakai, A. Frontera, S. Matile, Angew. Chem. Int. Ed. 57 (2018) 10883–10887.

[139] C. Wang, F.N. Miros, J. Mareda, N. Sakai, S. Matile, Angew. Chem. Int. Ed. 55 (2016) 14422–14426.

[140] A.-B. Bornhof, A. Bauzá, A. Aster, M. Pupier, A. Frontera, E. Vauthey, N. Sakai, S. Matile, J. Am. Chem. Soc. 140 (2018) 4884–4892.

[141] M. Akamatsu, N. Sakai, S. Matile, J. Am. Chem. Soc. 139 (2017) 6558–6561.

[142] K. Kapoor, M.R. Duff, A. Upadhyay, J.C. Bucci, A.M. Saxton, R.J. Hinde, E.E. Howell, J. Baudry, Biochemistry 55 (2016) 6056–6069.

[143] L. Adriaenssens, G. Gil-Ramírez, A. Frontera, D. Quiñonero, E.C. Escudero-Adán, P. Ballester, J. Am. Chem. Soc. 136 (2014) 3208–3218.

[144] Z. Rodriguez-Docampo, S.I. Pascu, S. Kubik, S. Otto, J. Am. Chem. Soc. 128 (2006) 11206–11210.

[145] P. Arranz-Mascarós, C. Bazzicalupi, A. Bianchi, C. Giorgi, M.-L. Godino-Salido, M.-D. Gutiérrez-Valero, R. Lopez-Garzón, M. Savastano, J. Am. Chem. Soc. 135 (2013) 102–105.

[146] Y. Marcus, G. HefterChem. Rev. 106 (2006) 4585–4621.

[147] J. Hernández-Trujillo, A. Vela, J. Phys. Chem. 100 (1996) 6524–6530.

[148] B. Jansik, D. Jonsson, P. Sałek, H. Ågren, J. Chem. Phys. 121 (2004) 7595–7600.

[149] E.F. Archibong, A.J. Thakkar, Mol. Phys. 81 (1994) 557–567.

[150] P. Calaminici, K. Jug, A.M. Köster, V.E. Ingamells, M.G. Papadopoulos, J. Chem. Phys. 112 (2000) 6301–6308.

[151] C. Hättig, O. Christiansen, S. Coriani, P. Jo/rgensen, J. Chem. Phys. 109 (1998) 9237–9243.

[152] S.K. Singh, A. Das, Phys. Chem. Chem. Phys. 17 (2015) 9596–9612.

[153] J. Hwang, P. Li, M.D. Smith, C.E. Warden, D.A. Sirianni, E.C. Vik, J.M. Maier, C.J. Yehl, C.D. Sherrill, K.D. Shimizu, J. Am. Chem. Soc. 140 (2018) 13301–13307.

[154] W.B. Motherwell, R.B. Moreno, I. Pavlakos, J.R.T. Arendorf, T. Arif, G.J. Tizzard, S.J. Coles, A.E. Aliev, Angew. Chem. 130 (2018) 1207–1212.

[155] I. Pavlakos, T. Arif, A.E. Aliev, W.B. Motherwell, G.J. Tizzard, S.J. Coles, Angew. Chem. Int. Ed. 54 (2015) 8169–8174.

[156] Santiago Alvarez, Dalton Trans. 2013, 42, 8617-8636.

[157] T.J. Mooibroek, P. Gamez, CrystEngComm 14 (2012) 1027-1030.

[158] B.P. Hay, R. Custelcean, Cryst. Growth Des. 9 (2009) 2539-2545.

[159] Anion Coordination Chemistry; Bowman-James, K., Bianchi, A., Garcia-España, E., Eds.; Wiley-VCH: New York, 2012.

[160] Sessler, J. L.; Gale, P. A.; Cho, W. S. Anion Receptor Chemistry; Monographs in Supramolecular Chemistry; RSC Publishing: Cambridge, U.K., 2006.

[161] ROKBOK Q.-H. Guo, Z.-D. Fu, L. Zhao, M.-X. Wang, Angew. Chem. Int. Ed. 53 (2014) 13548–13552.

[162] LIWFEE K. Liu, X. Han, Y. Zou, Y. Peng, G. Li, Z. Shi, S. Feng, Inorg. Chem. Commun. 39 (2014) 131–134.

[163] SUPGAN T.W. Myers, D.E. Chavez, S.K. Hanson, R.J. Scharff, B.L. Scott, J.M. Veauthier, R. Wu, Inorg. Chem. 54 (2015) 8077–8086.

[164] ZASSUJ K. Chainok, S.M. Neville, C.M. Forsyth, W.J. Gee, K.S. Murray, S.R. Batten, CrystEngComm 14 (2012) 3717–3726.

[165] QEZVIA C.S. Campos-Fernandez, R. Clerac, J.M. Koomen, D.H. Russell, K.R. Dunbar, J. Am. Chem. Soc. 123 (2001) 123, 773–774.

[166] NERQAE T.M. Klapotke, D.G. Piercey, F. Rohrbacher, J. Stierstorfer, Z. Anorg. Allg. Chem. 638 (2012) 2235–2242.

[167] FIZJIH C. Krieger, H. Fischer, F.A. Neugebauer, F. Guckel, D. Schweitzer, Acta Crystallogr. Sect.C: Cryst. Struct. Commun. 43 (1987) 1412–1415.

[168] JOYXEC H.-L. Vo, J.L. Arthur, M. Capdevila-Cortada, S.H. Lapidus, P.W. Stephens, J.J. Novoa, A.M. Arif, R.K. Nagi, M.H. Bartl, J.S. Miller, J. Org. Chem. 79 (2014) 8189–8201.

[169] C.S. Campos-Fernández, R. Clérac, K.R. Dunbar, Angew. Chem. Int. Ed. 38 (1999) 3477-3479.

[170] H.T. Chifotides, I.D. Giles, K.R. Dunbar, J. Am. Chem. Soc. 135 (2013) 3039−3055.

[171] L. Fritea, P. Audebert, L. Galmiche, K. Gorgy, A. Le Goff, R. Villalonga, R. Săndulescu, S. Cosnier, ChemPhysChem 16 (2015) 3695–3699.

[172] E. Garcia-España, P. Díaz, J.M. Llinares, A. Bianchi, Coord. Chem. Rev., 250 (2006) 2952–2986.

[173] H.-B. Liu, Q. Zhang, M.-X. Wang, Angew. Chem. Int. Ed., 57 (2018) 6536-6540.

Captions to Schemes

Scheme 1. The popular Pinner synthesis of symmetrically substituted *s*-tetrazines.

Scheme 2. Labeling of a biomolecule by a *tandem* process iedDA/rDA involving reaction of an alkene or alkyne dienophile connected to the biomolecule and a *s*-tetrazine bearing the label.

Scheme 3. Anion-π and lone pair-π interactions occurring with **2**-**5**. A, anion; Π, tetrazine; N, morpholine nitrogen; ln, lone pair; ~~, tetrazine-morpholine connector.

Captions to Figures

Figure 1. Relationships between molecular structural features, measurable properties and potential applications of *s*-tetrazine derivatives. a) LUMO of diphenyltetrazine according to ref [86]; b) Electrostatic potential of *s*-tetrazine, mapped onto the electron density isosurface, according to [100]; c) Depiction of positive quadrupole moment of s-tetrazine under polarization effected by an interacting anion.

Figure 2. Comparison of sampling areas of current and some recent CSD surveys on the matter. Visual analysis presented in the case of contacts between benzene and a Cl atom looking along a C-C-C benzene edge (black dots) in 1 Å : 1 cm scale (native artwork); a) [7]; b) [157]; c) [158], sampled area is internally limited to 1 Å thickness from the displayed ellipsoid to account for the excluded volume of the arene. Not showed for simplicity; d) present work; e) [26], sampled area is also duplicated under the ring plane. Not showed for simplicity.

Figure 3. Model of our CSD sampling routine, displayed as it would be for the search of contact between benzene and Cl atoms in 1 Å: 1 cm scale (native artwork) looking along a C-C-C side (black dots). Violet circle: generic spherical survey within 6.5 Å from the centroid; Blue circle: specific spherical survey at d_1(Cl) from the centroid. Orange square: hits falling within d_2(Cl) form the arene plane; only hits inside both the orange square and the blue circle are retained. Yellow circles: area within d_3(Cl) from at least one C atom of the ring; only hits in this area are evaluated in this paper. The same graph in the case of *s*-tetrazine (view along N-C-N side) would present two smaller yellow circles at the side, with a d_4(Cl) radius, accounting for the difference in vdW radii between C and N atoms.

Figure 4. Comparative representation of in-plane sampled areas for the benzene-chloride case between the model herein proposed (region touched by at least one of the yellow circles) and spherical or ellipsoidal sampling areas (red circle with r = 5 Å). Scale 1 Å : 1 cm (native artwork).

Figure 5. Coordinate reference system and main parameters used in this work to locate and discuss contacts around the *s*-tetrazine ring.

Figure 6. Global spatial distribution of anion contacts with the *s*-tetrazine ring reported as height (d plane) vs in plane displacement (d offset). All distances in Å.

Figure 7. Global angular distribution of anion contacts with the s-tetrazine ring reported as cumulative percentage of counts vs (bin centres of) angle. Bin size of the angle variable: 5°. Inset: graphical representation of hit distributions as a function of the angle at selected critical values.

Figure 8. Global spatial distribution of lone pair contacts with the s-tetrazine ring reported as height (d plane) vs in plane displacement (d offset). All distances in Å.

Figure 9. Global angular distribution of lone pair contacts with the *s*-tetrazine ring reported as cumulative percentage of counts vs (bin centres of) angle. Bin size of the angle variable: 5°. Inset: graphical representation of hit distributions as a function of the angle at selected critical values.

Figure 10. Distribution of anion (red) and lone pair (black) contacts with the *s*-tetrazine ring as a function of angle. Graph has been duplicated to show a 180° image. Experimental points are bridged by a spline. Bin size of the angle variable: 5°.

Figure 11. Hit distribution and approximate depiction of sampled areas showing the pits in hits density profiles observed for anionic (top) and lone pair-bearing species (bottom). Colour code: oxygen, red; nitrogen, blue; fluorine, orange. All distances in Å.

Figure 12. 2D-MIPp energy map of *s*-tetrazine interacting with F^- as a classical particle. Isocontour lines are shown every 5 kcal/mol and the global MIPp minimum is represented by a star. Reprinted from Ref. 105, with permission from Elsevier.

Figure 13. Hit distribution around the *s*-tetrazine ring for O anions (red) and lone pair bearing atoms. x and y are displacements along the respective axes. All distances in Å. a) view along the C-C axis; b) same view with stretched z axis allowing the appreciation of the potential well; c) 45° projection; d) view along the axis bisecting the N-N bonds. All distances in Å.

Figure 14. Projection of O anion (red) and lone pair (black) contacts with *s*-tetrazine in the xy plane. Approximate size of the *s*-tetrazine ring also shown for reference. All distances in Å.

Figure 15. Depiction of the ESP of the *s*-tetrazine molecule. Colour code: red -10 kcal/mol, blue +10 kcal/mol.

Figure 16. Projection of O anion contacts with s-tetrazine in the xy plane. Approximate size of the *s*-tetrazine ring also shown for reference. All distances in Å.

Figure 17. Projection of O lone pair contacts with s-tetrazine in the xy plane. Approximate size of the *s*-tetrazine ring also shown for reference. All distances in Å.

Figure 18. 3D wireframe diagram showing % contact distribution for O lone pair bearing atoms around *s*-tetrazine depending on their coordinates in the ring plane. All distances in Å. Bin size for the xy plane: 0.2 Å x 0.2 Å.

Figure 19. Top view of Figure 18, i.e. heat plot showing the hit density/localization probability for O lone pair bearing atoms around *s*-tetrazine as a function of the coordinates with respect to the ring plane. All distances in Å. Bin size for the xy plane: 0.2 Å x 0.2 Å.

Figure 20. 3D wireframe diagrams showing % contact distributions for O anions around *s*-tetrazine depending on their coordinates in the ring plane. All distances in Å. Bin size for the xy plane: 0.2 Å x 0.2 Å.

Figure 21. Top view of Figure 20, i.e. heat plot showing the hit density/localization probability for O anions around *s*-tetrazine as a function of the coordinates with respect to the ring plane. All distances in Å. Bin size for the xy plane: 0.2 Å x 0.2 Å.

Figure 22. Geometry of anion-π interaction with *s*-tetrazine-based ligand (3,6-bis[(morpholin-4-yl)ethyl]-1,2,4,5-tetrazine) for the series of halide anions. Bifluoride (HF_2^-) is the only example reported to date of anionic species featuring a charge-bearing F atom. Distances from the centroid (above) and offset values (under) are reported in Å. Reproduced from Ref. 73 with permission from The Royal Society of Chemistry.

Figure 23. Anion-π contacts between s-tetrazine moieties and chloride anions in the ROKBOK crystal structure (tetraethylammonium 2,7,12,17,22,27-hexaoxa-4,5,14,15,24,25,33,34,37,38,41,42-dodecaazaheptacyclo[26.2.2.23,6.28,11.213,16.218,21.223,26]dotetraconta-1(30),3,5,8,10,13,15,18,20,23,25,28,31,33,35,37,39,41-octadecaene chloride). Anion centroid unique distances 3.20, 3.12, 3.06 Å, offset 0.31, 0.21, 0.26 Å. [161]

Figure 24. The Ni(II)-based iodide binding scaffold of VAVSUH (tetrakis(m2-3,6-bis(2-Pyridyl)-1,2,4,5-tetrazine-N,N',N'',N''')-octakis(acetonitrile)-tetra-nickel(ii) iodide clathrate heptakis(hexafluoro-antimony). Anion-centroid unique distances 3.27, 3.52 Å, offset 0.0 Å in both cases. [125]

Figure 25. The Br_3^- interaction environment in VAVTES (tetrakis(m2-3,6-bis(2-Pyridyl)-1,2,4,5-tetrazine-N,N',N'',N''')-(acetonitrile)-heptabromo-tetra-nickel(ii) tribromide clathrate acetonitrile toluene solvate). Anion-π interactions with the central charge bearing Br atom respect ideal geometry (anion centroid distances 3.30, 3.34, 3.50, 3.52 Å, offset 0.08, 0.20, 0.19, 0.23 Å, respectively) while the lateral ones provide additional stabilization via off-centred anion-π contacts with the *s*-tetrazine moiety. [125]

Figure 26. Fragment of the LIWFEE crystal structure (catena-[bis(3,6-di(pyridin-4-yl)-1,2,4,5-tetrazine)-dinitrato-cadmium(ii) tetrakis(thiourea)-cadmium(ii) dinitrate]), featuring parallel stacks of strongly interacting *s*-tetrazine rings and nitrate anions. Angle between NO_3^- and *s*-tetrazine mean planes: 7.1°. [162]

Figure 27. Nitrate anion forming both parallel and perpendicular anion-π interactions with *s*-tetrazine in the Cu(II) complex of SUPGAN ((nitrato)-bis(3-(3,5-dimethyl-1H-pyrazol-1-yl)-6-(3,3-dinitroazetidin-1-yl)-1,2,4,5-tetrazine)-copper nitrate acetonitrile solvate). [163]

Figure 28. Top: apical (ZASSUJ, [164] catena-(bis(m2-3,6-di(pyrimidin-2-yl)-1,2,4,5-tetrazine)-di-silver(i) diperchlorate acetonitrile solvate)), lateral (VAVTAO, [125] tetrakis(m2-3,6-bis(2-Pyridyl)-1,2,4,5-tetrazine-N,N',N'',N''')-tetrakis(acetonitrile)-tetra-aqua-tetra-nickel(ii) perchlorate clathrate heptakis(periodate) acetonitrile solvate)) and facial (ASUNAF, [71] 4,4'-[1,2,4,5-tetrazine-3,6-diyldi(ethane-2,1-diyl)]bis(morpholin-4-ium) diperchlorate monohydrate) anion-π interaction of *s*-tetrazine with perchlorate anions. Bottom: scheme of the three different interaction geometries.

Figure 29. Discrete self-assembled molecular pentagon as observed in QEZVIA (pentakis(m2-3,6-bis(Pyrid-2-yl)-1,2,4,5-tetrazine-N,N',N'',N''')-decakis(acetonitrile-N)-penta-nickel(ii) hexafluoro-antimony clathrate nonakis(hexafluoro-antimony) acetonitrile solvate). [165]

Figure 30. a) Distribution of water molecules O around the *s*-triazine core; b) orientation of water molecules around the *s*-triazine core showing convergence of H atoms towards the H-bond acceptor N, and of O atoms towards the ring centroid, in a lone pair-π-type interaction; c) Distribution and orientation (halved on molecular symmetry plane) of generic C=O functions around *s*-triazine core showing the tendency to direct the O end of the carbonyl group towards the ring centroid. Displayed molecules are in contact within the sum of vdW radii. Generated using Isostar.

Figure 31. NERQAE (catena-[(m4-5,5'-(1,2,4,5-Tetrazine-3,6-diyl)bis(tetrazolido))-tetrakis(m2-aqua)-di-sodium(i) dihydrate]), ideal lone pair-π interaction between *s*-tetrazine and water (a), or just water molecules filling voids in the hydrophilic channels of a MOF-like structure (b)? [166]

Figure 32. Strong and centred O lone pair-π interaction as observed for 3,6-bis[(morpholin-4-yl)methyl]-1,2,4,5-tetrazine in DETNAU (O¨¨centroid 2.96 Å, offset 0.15 Å, angle 86.9°).[73]

Figure 33. Strong and centred N lone pair-π interaction as observed for 3,6-bis[(morpholin-4-yl)ethyl]-1,2,4,5-tetrazine in DETNEY (N···centroid 3.24 Å, offset 0.18 Å, angle 88.9°). [73]

Figure 34. Structural features of 3,6-bis(1-Aziridinyl)-1,2,4,5-tetrazine in the FIZJIH crystal structure. The overall crystal packing (a) seems to be due to an offset π-π stacking interaction pattern, but close inspection reveals little to no superimposition of aromatic rings (b). The main interaction appears to be due to lone pair-π contacts (c) (N…centroid 3.12 Å, offset 0.18 Å, angle 86.7°). [167]

Figure 35. Structural features of JOYXEC: overall crystal packing (a) and details of lone pair-π contacts (b) (N…centroid 2.83 Å, offset 0.20 Å, angle 85.9°). [168]

Figure 36. Molecular structure of $[Ni_4(bptz)_4(CH_3CN)_8]^{8+}$ with the encapsulated BF_4^- anion [169].

Figure 37. Highlights of the prominence of anion-π interactions in the complexes of the diprotonated homologous ligands **2**-**5**. [71-75]

Figure 38. Equilibrium constants (K) for the reactions $H_2L2^{2+} + X^- = [(H_2L2)X]^+$ (X = halide). For Cl^-, K was arbitrarily set equal to zero, as it is expected to be close to this value. Reproduced from Ref. 73 with permission from The Royal Society of Chemistry.

Figure 39. Computed structures of anion-π complexes $[(\mathbf{6})N_3]^-$ (a) and $[(\mathbf{9})N_3]^-$ (b) with top (left) and side (right) views. Reproduced from Ref. 173 with permission from Wiley-VCH.

Supplementary material

for

Anion-π and lone pair-π interactions with *s*-tetrazine-based ligands.

Matteo Savastano,[a] Celeste García-Gallarín,[b] Maria Dolores López de la Torre,[b] Carla Bazzicalupi,*[a] Antonio Bianchi,*[a] Manuel Melguizo*[b]

[a] Department of Chemistry "Ugo Schiff", University of Florence, Via della Lastruccia 3, 50019 Sesto Fiorentino, Italy

[b] Department of Inorganic and Organic Chemistry, University of Jaén, 23071 Jaén, Spain

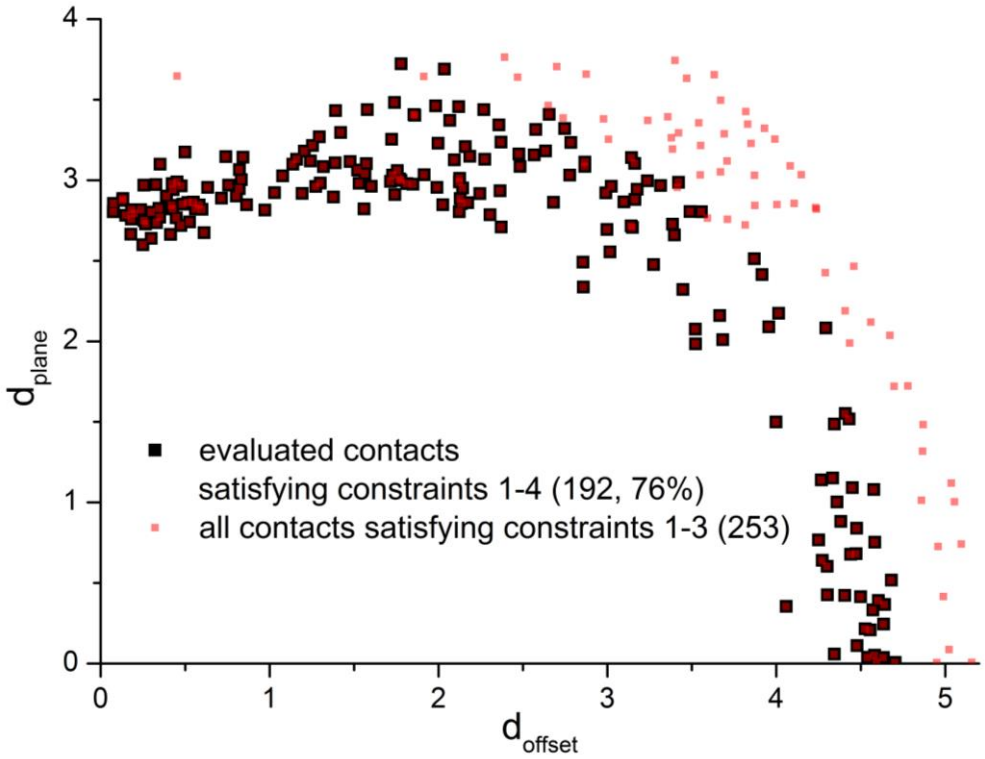

Figure S1. Distribution of contacts around the tetrazine ring for oxygen lone-pair bearing atoms of the =O type connectivity. The evaluated contacts satisfying all 4 criteria (in black) are only the 76% of those satisfying criteria 1-3. Red contacts do not bear chemical significance. Even contacts located in the area above the centroid may be excluded if they do not satisfy the specified parameters (i.e. we are not biasing toward the centroid). All distances in Å.

A Note on Formalism

The Conquest formalism will be used in the following discussion for atoms, bonds, connectivity, charges and so on, in order to make the searches easily reproducible and allow the quick extension of the methodology to other systems.

A reference key is given below.

Atom types:

Elements	as usual
Any	X
Any halogen	7A

Bond types:

Single, double and triple bonds:	as usual
Aromatic:	═ ═ ═
Any (undefined):	– – – –

Charge:

Defined positive / negative:	+# / -#
Any (undefined) positive:	+ve
Any (undefined) negative:	-ve
Zero:	0ve

Number of bonded atoms:

For # bonded atoms (e.g. 2):	T# (e.g. T2)

Other Objects:

Centroid will be here displayed as a blue dot. 

Searched Contacts will be here displayed as a dashed red line. – – – –

These items are highlighted differently in Conquest.

Evaluating Contacts: the Problem of Distinguishing Anions and Lone Pairs in Conquest

As any software, Conquest is no chemist. Therefore, it will do exactly what it is required to do by the user: no questions asked, no quarters given.

As a first example we will consider oxyanions.

One may think that to locate all oxyanions within a certain distance from the centroid of an *s*-tetrazine a query like the one reported below may suffice.

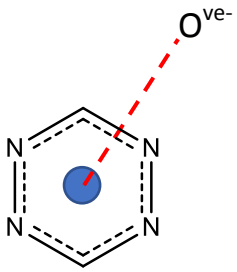

Instead, this query is flawed and will result in the mixing between anion and lone pair results. Why?

To understand it, let us take a look at perchlorate, a classic oxyanion.

Conquest would draw perchlorate this way:

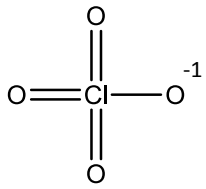

It has no notion of delocalization and equivalence of the 4 oxygen atoms, instead it thinks it knows exactly (from crystal data and bond lengths) the single oxygen atoms which bears the negative charge. This may seem a mere formalism, yet the above query will count a hit only if the oxygen atom which formally bears the charge is found in contact with the centroid, the other 3 oxygen atoms do not correspond to the search criteria.

Moreover, the other three oxygen atoms will show up as lone pair bearing atoms (and not anions) in the lone pair search, done with the same criteria but specifying that oxygen should bear a 0 net charge, showed

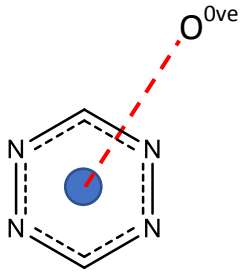

below.

This would end up mixing anion and lone pair contacts query results.

A proper way to cope with these problems is to perform a screen of the type of oxyanions which are found interacting with tetrazine in the CSD.

Then use a type by type search. For perchlorate an appropriate one would be:

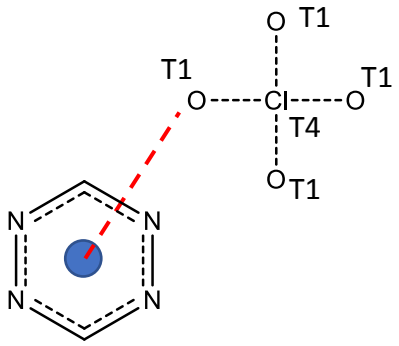

This will actively locate all the contacts with perchlorate we may be interested in. Moreover, it will actively exclude all systems in which the oxygen tips of the anion are bound to something else, which is useful to discriminate metal bonded systems whose geometry may differ considerably.
But how can we make sure that these same contacts will not be counted also as lone pair-π contacts of the X=O type?
A fast approach to the problem is combining two queries with a Boolean NOT function. This can be handled easily by Conquest and will result in accurate sampling. A possible correct query for X=O lone pairs would be:

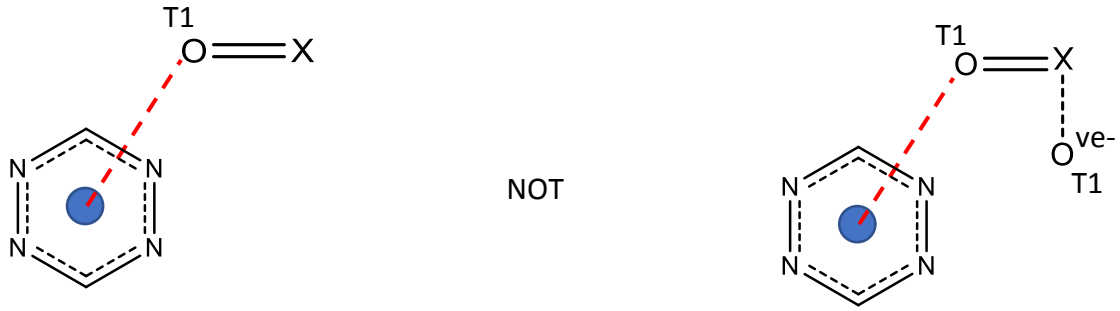

where we require that to be included in the hits the contact must possess the structural feature shown on the left but not the one shown on the right.
The quick extension to all oxyanions is then straightforward. Unluckily this does not exhaust the most common fallacies.

Let us now consider anions where fluoride is the atom in contact.
As before, when looking for contacts with these species one is tempted by the simplicity of this query:

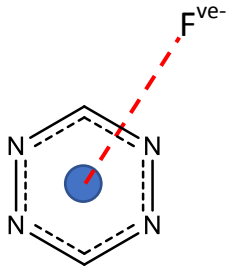

This however will only locate fluoride anions, while species like BF_4^- and AF_6^- (A = P, As, Sb) will not be searched for. The reason is simple: the negative charge is formally not on F, but, as the names of these

anions suggest (-ate), it is on the central atom. Moreover, all the tetra and hexafluoro anions risk to be included in the number of lone pair-π contacts. Additionally, if pnictogen anions were common, we would risk, for example, to include hexafluorophosphate in the number of phosphide type anions.
Accordingly, each of these searches requires special attention.
For anions, it is sufficient to draw them more explicitly as F-X (X any but 7A, see below) and specify that X must bear a negative net charge.
For lone pairs of the X-F type, it is necessary to specify that X must bear a 0 net charge.
This kind of issues may cause errors in evaluating contacts, specifically affecting the atom from which the contact is measured. This is the reason why in Table 2 entries are reported according to "Atom in Contact" and not "Charge-bearing Atom". In PF_6^-, for example, the charge bearing atom would be P, but measuring contacts from P will not account meaningfully for the interactions; instead the contacts should be measured between centroid and F atoms, thus using search criteria accounting for the size of F and not for the radius of P.

The above also applies to the other halide anions, but with some twists.
As another example, it should be noted that searches like Cl-X with X bearing a negative net charge, will locate among the tetra and hexachloro species also perchlorate (X = O), with the contacts measured from chloride this time, which naturally do not represent a meaningful result and should be excluded.

Another peculiar case is that of interhalogen anions. These may result in ambiguities due to the fact that, given a certain anion, the atom in close contact with the centroid may or may not be the one formally bearing the negative charge. On the other hand, when looking for lone pairs in the form of X-7A, the two terminal atoms of an $7A_3^-$ anion (eg. I_3^-) will be considered as lone pairs by Conquest (this is true also for interhalogen anions of higher atomicity).
One of the best approaches goes as follows: for anions, locate all contacts with monoatomic halides anions (specifying 0 bonded atoms, T0, and negative net charge); for lone pairs, use a Boolean NOT function to exclude hits with 7A-7A bonds when looking for 7A-X lone pairs; then search explicitly for 7A-7A interacting species and sort them out by hand.

As you should have realized by know, all of this requires thinking according to strict formalism and double checking that everything is working as intended, that all species are included, counted only once and measured from a meaningful interacting atom.

Handling of 3D Data: Methodology, Assumptions, Corrections

3D data can be freely extrapolated from the atom to atom distances measured by Conquest.

There may be better or different approaches to it, however this kind of procedure is rarely done by hand, the more so nowadays as Isostar will perform it automatically for the implemented systems (most likely with a far more efficient algorithm).

However, in our opinion it is instructive to show how this can be done freely by anybody with a simple spreadsheet. In second instance, one cannot fully appreciate the manual control and the understanding that this gives on the data until one experiences it. Finally, some non-trivial stratagems must be implemented to make sure that Conquest or mathematical treatment do not tamper with the data.

The problem is finding {x,y,z} Cartesian coordinates (polar ones can be as fine) of the anion in contact measuring only distances from meaningful Conquest objects (atoms, centroid and mean plane).

The z problem is non-existent: if we pick the xy plane as the mean ring plane we can measure z straight away.

For the other 2 parameters the methodology *per se* is extremely simple, involving Pythagoras' theorem (others could be used, especially if we wanted to focus on some of the angles). Yet a few focal points should be discussed.

Before discussing the methodology, we should consider 3 facts:

1) If we refer to the centroid alone (measuring the anion-centroid distance) we will never be able to locate the anion (a given distance from a point only defines a sphere); this means that we need to get some other parameters and refer to more than one physical point from which we can measure distances (i.e. we will need to measure distances also from some atoms in the ring);
2) *s*-terazines are symmetric. This tells us that all of our data will fall in one octant of Cartesian space, which was replicated in the displayed results in the review to produce a full image (more on this concept below). Moreover, symmetry strongly suggests orienting the reference system to have one Cartesian axis oriented along the C-C molecular axis;
3) Numbering. We can ask Conquest to measure distances from N1 and C3, but how do we know if the addressed atoms are really the ones that we mean? Let us discuss this from the carbon viewpoint first. When *s*-tetrazine retains its own symmetry and the numbering is arbitrary (i.e. C3 could be C6 from a chemical standpoint), if we measure the C3-anion distance how do we know which one of the carbon atoms the program will choose? This matters for our scope, because C3-anion and C6-anion distances are going to be generally different. Moreover, what if the tetrazine lowers its symmetry due to substituents? Then we could really tell the difference between C3 and C6, but how can be sure of which one is picked?
   Remember that a query will look like this, so nothing is specified about C substituents.

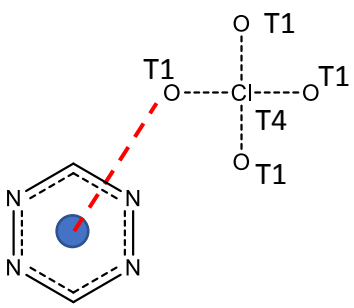

As you can imagine, nitrogen is even a worse choice, we end up having ambiguity between 4 atoms instead of 2.

We will now provide a solution for the geometric problems which accounts for the above remarks.

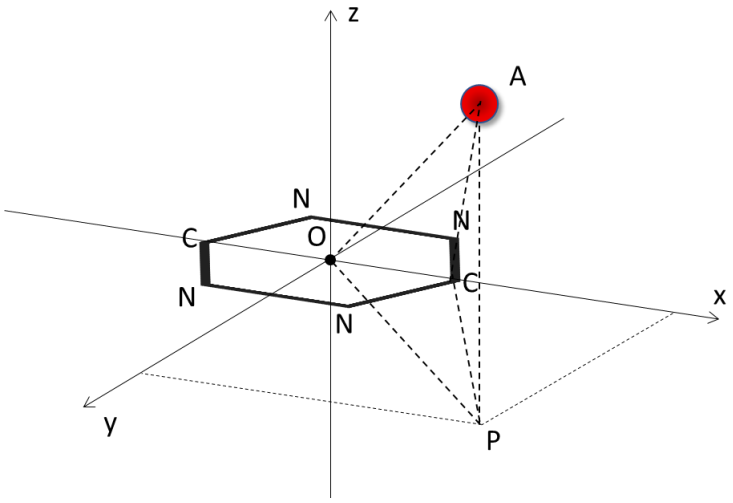

The geometry of the problem is as follows:
O origin of the reference system and Centroid position
A position of the Anion
P Projection of A in the xy plane
xy plane coincides with ring mean plane
x axis coincides with CC axis
AO = Anion Centroid distance
OP = Offset

Since P is the orthogonal projection of A in the xy plane, any generic Q point belonging to xy will form a QPA 90° angle.
From the above we may state that also CPA is 90° and therefore we can write the following equation (Pythagoras' theorem):

$$CP = \sqrt{CA^2 - AP^2}$$

This may seem a worthless result, however we just managed to measure CP, which is non-directly accessible (P is not a physical point from which Conquest may measure distances) from 2 measurable quantities: CA and AP (measured as A distance from the ring mean plane).
This warns us of the only approximation used to generate the 3D distributions: the ring plane should be a "good plane" (see below), i.e. the s-tetrazine ring must not significantly deviate from planarity. If that happens CPA may not be right-angled, Pythagoras theorem is not applicable and simple math gets messed up (see below).
Let us now move from the 3D system to the xy plane (z coordinate is trivial and has been addressed above).

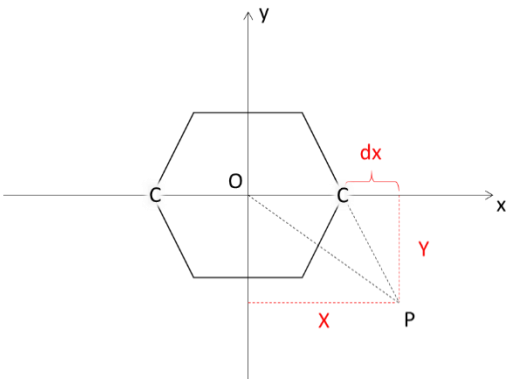

Case 1

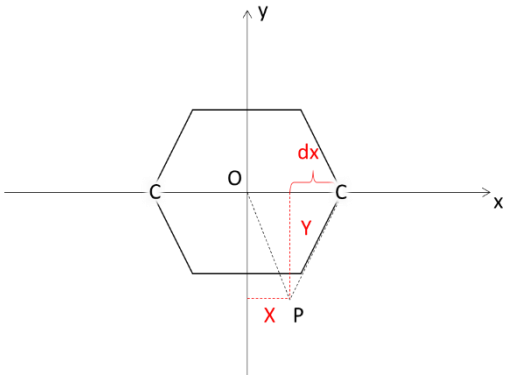

Case 2

where X and Y are the {x,y} Cartesian coordinates searched for and dx is the absolute difference between X and OC segment lengths.

Although looking different, both cases can be solved with the same equations (due to the quadratic dependence of the solution).
Solution of the system goes as follows.

Case 1

$$\begin{cases} OC + dx = X \\ X^2 + Y^2 = OP^2 \\ dx^2 + Y^2 = CP^2 \end{cases}$$

Case 2

$$\begin{cases} OC - dx = X \\ X^2 + Y^2 = OP^2 \\ dx^2 + Y^2 = CP^2 \end{cases}$$

From which:

$$\begin{cases} dx = X - OC \\ Y^2 = OP^2 - X^2 \\ dx^2 + Y^2 = CP^2 \end{cases}$$

$$\begin{cases} dx = OC - X \\ Y^2 = OP^2 - X^2 \\ dx^2 + Y^2 = CP^2 \end{cases}$$

Substituting the firs two equations in the third one:

$$X^2 - 2OC\,X + OC^2 + OP^2 - X^2 = CP^2$$

Then:

$$X = \frac{OC^2 + OP^2 - CP^2}{2OC}$$

This solves the systems, allowing to calculate X and then Y according to $X^2 + Y^2 = OP^2$.

Let us know discuss the critical points of the methodology.

CP

Two different CP values exist for each ring as there are two carbons (C3 and C6). Since numbering is an issue, the safest procedure is to measure both C3P and C6P and use the shortest one. This will automatically reduce the problem to the closest carbon to the anion, which is perfectly coherent with the symmetry of the s-tetrazine, which forces reduction of the problem to a single octant anyway.

OC

Any attempt to use OC average value for s-tetrazine (1.28 ± 0.02 according to Conquest) resulted in poor results. It is obvious that the imperfect quantification of the OC distance results in a slight alteration of the distribution. Beyond fidelity issues, that would not be much of a problem (overall the distribution would remain similar), most of the problem comes from the fact that non-exact OC distances may result at times in a sign switch: a single negative root would prevent the localization of the point in a cascade fashion in a spreadsheet (square roots from Pythagoras' theorem are bound to fail on negative numbers). For these reason OC3 and OC6 have been directly measured in Conquest for each hit when generating datasets for 3D graphs. Provided that within a single hit evaluation the numbering of Conquest is consistent, we can then find out the correct carbon atom by the difference in CP values (C3P or C6P, see above) and then select the correct OC value to use (OC3 and OC6). Case by case, numbering is unambiguous and will result in maximum accuracy. Presented results have been obtained in this way.

For performing this procedure in a spreadsheet, simple differences and spreadsheet sorting are first choice tools.

“Bad data”: “Bad Math” and “Bad Plane”

Planarity is the only weak spot of the methodology. When the tetrazine is not planar the mean plane might not be reliable and alter results. If in most cases (when the deviation is small) this causes a slight shift in {x,y,z} coordinates, in some cases this may totally prevent the localization of the anion: this happens when one of the derived distances turns negative. We dubbed this kind of behaviour as “bad data”. On our datasets this has a low percent incidence (1-5 % depending on the dataset). However, we noticed that dubbing these faulty data as “bad data” is not the most correct procedure. Indeed, some of these data are indeed ascribable to “bad plane” type problems, since there are no other reasons for the procedure not to work. Conversely the other part of “bad data” were found not to be defective *per se*, but more susceptible to the data handling procedure: these data were dubbed as “bad math” (see below) and reintroduced in the final graphs. In this way we managed to recover 20-50 % (depending on dataset) of the contacts which could not be localized in 3D at first, limiting them to real “bad plane” data, which are not in a sufficient number to modify the 3D distributions.

What is the nature of the so called “bad math” problems?

Provided that mathematics is in truth totally fine, they have to do with the robustness of the equations towards minor planarity problems, which are relevant in 2 distinct limit cases: x = 0 and y = 0.

In a general case, generic true coordinates, e.g. {3, 2}, could be slightly modified (randomly) by an imperfect planarity and evaluated for example as {2.95, 2.03}. This would have overall no net effect on the distribution. What is important to notice is that the equation system is generally robust towards deviation from planarity: it will produce less accurate depictions, but the roots will stay meaningful and positive.

For points like {0, y} or {x, 0} chance is that the effect of planarity issues would be turning negative one of the coordinates, which implies that one of the square roots will fail and the point will not be represented in the final diagram.

To solve this kind of issues two checks have been performed and tolerance values have been set.

In the case of x = 0, it was checked if C3A and C6A (distances within each of the carbon atoms and the anion) were found equal (by taking their difference). When their difference is 0 the point really lies on the y axis and the fact that we do not find x = 0 means that deviation of planarity makes it switch sign. This still holds when C3A and C6A are not perfectly equal (since we are considering an issue of deviation from ideal geometry), therefore an arbitrary threshold value for their difference should be included. We decided that “bad data” displaying a negative x value and C3A-C6A absolute difference below 0.05 Å could potentially be “bad math” data. In those cases, data were corrected by setting x = 0, calculating the corrected y, and, if that resulted in a positive root, re-added to the final graphs.

In the case of y = 0, the projection of the anion should lie on the x axis. If that is the case, offset value and x value should coincide. Once more, if OP (offset) and x absolute difference was found to be within 0.05 Å, data were adjusted according to y = 0 and added to the final graphs.

The remaining “bad data” have a truly poor ring planarity. We may argue if coincidence of the anion projection on the xy plane P with the in-plane coordinate of one C atom, would be another dangerous case

easily preventing CP calculation. However, CP correction (x = OC, i.e. P and C coincide) does not generally results in any improvement of the data, as y calculation also tends to fail. This is because failure of CP calculation in the first place indicates that CA (the anion-carbon distance) is greater than AP (the anion-mean plan distance): if the carbon atom belonged to the xy plane this should not be possible (i.e. the shortest point to plane distance must be along the normal to the plane passing for the point), hence we are really in the presence of deviation from ideal geometry that cannot be easily remediated.

As stated above, this affects only small percentage of data, so please bear in mind that all of this has very limited consequences on the reported distributions and all cares to minimize its effect and produce high-fidelity images of the distributions have been taken.

Finally, in principle these problems could be avoided. A possible solution would be defining 2 additional planes beyond the ring mean plane. For example, we could consider the mean plane of ring atoms 1 3 and 5 and that of atoms 2 4 and 6 and ask that the angle between these two planes is below an arbitrary threshold. This query can be carried along with a Boolean AND function and would generally improve data quality. Due to the reduced number of available structures this was not done for s-tetrazine. However, this is recommended for highly represented systems in the CSD (number of hit beyond 500000 are commonplace for benzene, in that case this additional criterion becomes an optimum data quality/quality of life solution).

Data Representation

As said above, true data belongs to a single octant of Cartesian space. Displayed graphs are mirrored to reproduce the distribution above one face of the tetrazine. One may feel that this is a trick to actively multiply available data by 4.

This is not the case. It is true that the white portion of the graph below carries all the information, yet this kind of data presentation lacks immediacy. One is not able to tell how the overall distribution will look nor to appreciate properly contact rich areas.

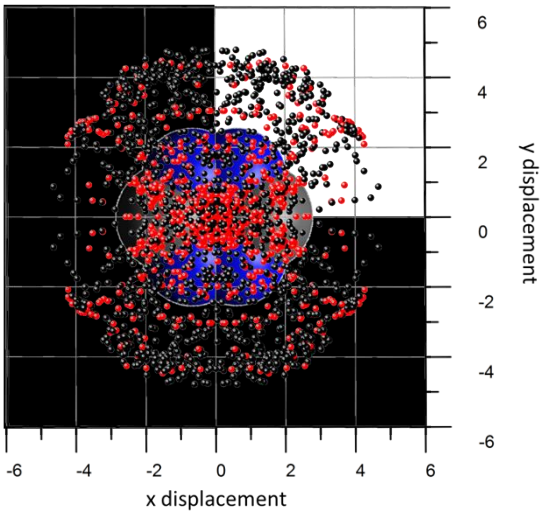

Conversely, the darkened mirrored picture may not contain any additional information, yet it allows to understand far better the meaning of the distribution.

Moreover, this kind of problems exist for the vast majority of heterocycles, and also widely accepted tools like Isostar use molecular symmetry to depict complete distributions around a fragment. Symmetry considerations have long been a cornerstone of Science and could not be more widely accepted. The only

important things in our context are understanding the overall distribution pattern and remembering that only a portion of it corresponds to real contacts, while the rest is symmetry generated.